HAL
open science

Detailed experimental and kinetic modeling study of toluene/C2 pyrolysis in a single-pulse shock tube

Wenyu Sun, Alaa Hamadi, Said Abid, Nabiha Chaumeix, Andrea Comandini

To cite this version:

Wenyu Sun, Alaa Hamadi, Said Abid, Nabiha Chaumeix, Andrea Comandini. Detailed experimental and kinetic modeling study of toluene/C2 pyrolysis in a single-pulse shock tube. Combustion and Flame, 2021, 226, pp.129-142. 10.1016/j.combustflame.2020.11.044 . hal-03058325

HAL Id: hal-03058325

https://hal.science/hal-03058325v1

Submitted on 11 Dec 2020

HAL is a multi-disciplinary open access archive for the deposit and dissemination of scientific research documents, whether they are published or not. The documents may come from teaching and research institutions in France or abroad, or from public or private research centers.

L'archive ouverte pluridisciplinaire **HAL**, est destinée au dépôt et à la diffusion de documents scientifiques de niveau recherche, publiés ou non, émanant des établissements d'enseignement et de recherche français ou étrangers, des laboratoires publics ou privés.

Combustion and Flame 226 (2021) 129–142

Contents lists available at ScienceDirect

Combustion and Flame

journal homepage: www.elsevier.com/locate/combustflame

Detailed experimental and kinetic modeling study of toluene/C_2 pyrolysis in a single-pulse shock tube

Wenyu Sun[a,*], Alaa Hamadi[a], Said Abid[a,b], Nabiha Chaumeix[a], Andrea Comandini[a,*]

[a] CNRS-INSIS, I.C.A.R.E., 1C, Avenue de la recherche scientifique, 45071 Orléans cedex 2, France
[b] Université d'Orléans, 6 Avenue du Parc Floral, 45100 Orléans, France

ARTICLE INFO

Article history:
Received 17 September 2020
Revised 27 November 2020
Accepted 27 November 2020

Keywords:
Toluene
Acetylene
Ethylene
Single-pulse shock tube
Polycyclic aromatic hydrocarbons (PAHs)

ABSTRACT

A combined experimental and kinetic modeling study is carried out to explore the influences of acetylene and ethylene addition on the species formation from toluene pyrolysis. Experiments are conducted separately with four different argon-diluted binary toluene/C_2 mixtures in a single pulse shock tube at a nominal pressure of 20 bar over a temperature range of 1150−1650 K. All the experimental mixtures contain about 100 ppm toluene and different amounts of C_2 fuels (50, 216, 459 ppm acetylene and 516 ppm ethylene). Species concentrations as a function of the temperature are probed from the post-shock gas mixtures and analyzed through the gas chromatography/gas chromatography-mass spectrometry techniques. A kinetic model is developed, which successfully predicts the absolute species concentration measurements as well as the changes brought by the varied fuel compositions. With the neat fuel decomposition profiles as a reference, both fuel components exhibit increased reactivity in the pyrolysis of all studied binary mixtures, indicating the existence of obvious synergistic effects. In particular, such effects become more remarkable when increasing the initial acetylene concentration. This essentially results from the addition-elimination reaction of a toluene fuel radical and a C_2 fuel molecule leading to a C_9 molecule and a hydrogen atom. Indene is identified as the predominant C_9 product in all studied cases, and its peak concentrations sharply increase with the initial acetylene contents in toluene-acetylene pyrolysis. On the other hand, indane, produced from the addition-elimination reaction between benzyl and ethylene, is only detected at trace levels in toluene/ethylene pyrolysis. This indicates a relatively weaker interaction between benzyl and ethylene, compared to that of benzyl and acetylene. Apart from the increased concentrations of hydrogen atoms and C_9 aromatics, interactions between toluene and C_2 fuels also directly result in a reduced level of C_7 radicals in the reaction system. Overall, PAH species can be divided into two groups according to the way their peak concentrations varying with the initial fuel compositions. For those largely depending on benzyl reactions, such as bibenzyl, biphenylmethane, fluorene and phenanthrene, the peak concentrations decrease with the added C_2 fuels. In contrast, increasing trends are observed in the peak concentrations of the PAHs which rely on indenyl as a precursor, including naphthalene, methyl-indene, benzofulvene and acenaphthalene.

© 2020 The Author(s). Published by Elsevier Inc. on behalf of The Combustion Institute.
This is an open access article under the CC BY-NC-ND license
(http://creativecommons.org/licenses/by-nc-nd/4.0/)

1. Introduction

Being found as the most predominant aromatic in gasoline, toluene serves as an essential component of the ternary (*n*-heptane/iso-octane/toluene) surrogate fuel mixtures that are widely formulated and utilized in the last decade [1]. Given such importance, a wealth of studies were carried out to establish the kinetic mechanism responsible for toluene consumption under combustion relevant conditions. Available experimental data cover global parameters such as ignition delay time [2,3], laminar burning velocity [4] and detailed species compositions in jet-stirred reactor oxidation [5-7], premixed flames [8,9] and flow-reactor [7] or shock tube [10-12] pyrolysis. The decomposition of toluene produces various resonantly stabilized radicals such as benzyl, fulvenallenyl, cyclopentadienyl and propargyl. Reactions of these radicals among themselves [13-16] or with other abundant combustion radicals/molecules [17-19] are identified as important pathways leading to polycyclic aromatic hydrocarbon (PAH) compounds. Accurate kinetic characterization of relevant channels need to be

* Corresponding authors.
E-mail addresses: wenyu.sun@cnrs-orleans.fr (W. Sun), andrea.comandini@cnrs-orleans.fr (A. Comandini).

https://doi.org/10.1016/j.combustflame.2020.11.044
0010-2180/© 2020 The Author(s). Published by Elsevier Inc. on behalf of The Combustion Institute. This is an open access article under the CC BY-NC-ND license (http://creativecommons.org/licenses/by-nc-nd/4.0/)

included in developing predictive combustion kinetic models of PAH formation, and such models are fundamental in numerical designs towards new clean combustion strategies.

Simple C_2 hydrocarbons, acetylene (C_2H_2) and ethylene (C_2H_4) are usually abundant intermediates in practical combustion systems. The decomposition of C_2 species and the build-up of larger hydrocarbons under pyrolytic conditions is a classical topic and has been long-studied in the combustion kinetics community [20-31]. The interactions between C_2 and aromatic radicals, for instance, the well-known Hydrogen-Abstraction-C_2H_2-Addition (HACA) routes [32,33], play a vital role of PAH formation and growth. More specifically, the interaction between C_2H_2 and benzyl is deemed as an important source of indene, and the rate coefficients of relevant reactions have been derived through theoretical calculations [18,34]. Toluene pyrolysis, especially with the presence of C_2H_2, can provide ideal environments to inspect these reaction channels. The pyrolysis of toluene-C_2H_2 was studied in a few previous works through experimental and kinetic modeling approaches. Shukla et al. [35] compared the PAH products from neat toluene and toluene/C_2H_2 pyrolysis in a low-pressure flow reactor by using in-situ direct sampling mass spectrometry technique. They suggested relevant PAH formation schemes based on the products mass spectra, though no quantitative measurements were obtained [35]. Later, a kinetic model was proposed by Matsugi and Miyoshi [36] to interpret two- and three-ring PAH formation from the pyrolysis of toluene and toluene-C_2H_2 mixtures, and the model could satisfactorily predict the qualitative experimental observations in [35]. Very recently, Li et al. [37] investigated the co-pyrolysis of toluene and C_2H_2 in a flow reactor at atmospheric pressure over 1057–1340 K. Mole fractions of crucial species concentrations were measured via a photoionization mass spectrometer. Through comparisons with the cases of neat toluene and neat C_2H_2 pyrolysis, Li et al. [37] pointed out that in toluene and C_2H_2 co-pyrolysis, the decomposition of both fuels is greatly stimulated. Such phenomena were explained with a circulating reaction sequence converting toluene+C_2H_2 to indene and H_2 [37]. The work by Li et al. [37] focused on the synergistic effects of fuel decomposition, so only limited PAH speciation measurements were reported. However, the interactions between toluene and C_2H_2 can directly or indirectly alter the PAH formation scheme. This subject merits further investigations, in particular, at elevated pressures that are more relevant to practical conditions. Furthermore, by varying the initial fuel composition, *i.e.* the proportion between toluene and C_2H_2, the reliability of kinetic parameters for important channels can be examined under reaction environments containing different chemical compositions. Though C_2H_4 is also a crucial combustion intermediate, how it reacts with aromatic radicals received relatively less attention. Our recent work [38] showed that C_2H_4 and C_2H_2 have different influences on the formation of PAHs, specifically, naphthalene and acenaphthalene, from phenylacetylene pyrolysis. Definitely, valuable insights can be acquired by exploring the interactions between C_2H_4 and radicals produced from toluene pyrolysis and by comparing the different effects of C_2H_2 and C_2H_4.

To this end, two major goals are concerned in the current study: i) compare the effects of adding C_2H_2 and C_2H_4 to toluene pyrolysis, regarding the fuel decomposition reactivity and the directly or indirectly affected speciation behaviors; ii) track and account for the variation trends of crucial PAH concentrations when adding different amounts of C_2H_2 to toluene pyrolysis. Shock tube pyrolysis experiments are carried out with different toluene/C_2H_2 (C_2H_4) mixtures having the same amount of toluene but varying C_2 contents. Species concentrations that evolve with the post-shock temperature are obtained via the gas chromatography/gas chromatography–mass spectrometry (GC/GC–MS) technique. A kinetic model is developed by incorporating the reactions between C_2H_x and toluene related species. Through a combination of experimental measurements and modeling analyses, the addition effects of C_2 fuels on toluene consumption, as well as the further impacts on PAH speciation will be illustrated.

Table 1
Compositions of the gas mixtures used for experiments.

Composition	Gas mixture		
	Toluene (C_7H_8)	Ethylene (C_2H_4)	Acetylene (C_2H_2)
TE	106 ppm	516 ppm	–
TA_50	107 ppm	–	50 ppm
TA_216	106 ppm	–	216 ppm
TA_459	105 ppm	–	459 ppm

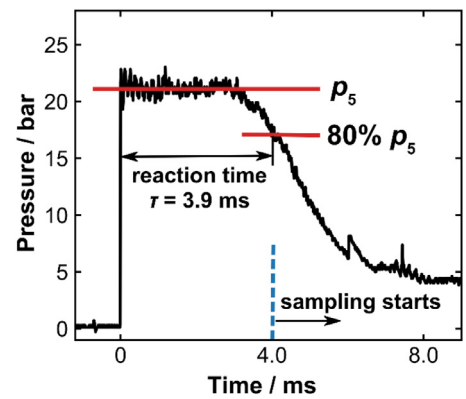

Fig. 1. A measured endwall pressure history and the definition of the reaction time.

2. Shock tube pyrolysis experiments

The experimental work is carried out with the single-pulse shock tube facility at ICARE, Orléans, France. Detailed descriptions about the shock tube apparatus and the coupled gas chromatography/gas chromatography–mass spectrometry (GC/GC–MS) diagnostic technique can be found in our previous publications [12,38,39]. Briefly, the driven (78 mm in inner diameter and 6.0 m in length) and driver sections are separated by a double diaphragm. To operate the shock tube in a single-pulse fashion, a dump tank, with a volume five times bigger than the driven section, is placed near the diaphragm on the driven section side. The driven section is heated up at 90 °C to prevent the condensation or absorption of fuels and reaction products on the shock tube inner surface. Four argon diluted binary fuel mixtures are used in the current experiments, including one toluene-ethylene mixture and three toluene-acetylene mixtures with different acetylene contents. The detailed compositions of the experimental mixtures are listed in Table 1.

Four pressure sensors (CHIMIE METAL A25L05B) are mounted along the sidewall of the driven section at intervals of 150 mm, with the last one being 82 mm away from the endwall. The time when the shock wave passes individual sensors is recorded to derive the incident shock velocity. The post-shock conditions (p_5 and T_5) is subsequently determined by solving conservation equations together with the ideal gas law and variable heat capacity ratio. The uncertainty of the calculated T_5 is estimated to be ±30 K, mainly due to the uncertainty in the determination of the actual positions of the pressure sensor sensitive surfaces. Such spatial uncertainties are estimated to be 2 mm, equal to the sensor diameter. A PCB Piezotronics pressure sensor shielded by a layer of room-temperature vulcanizing (RTV) silicone is placed on the endwall. One of the recorded endwall pressure histories is shown in Fig. 1, and the corresponding reaction time is defined as the interval between the arrival of the shock wave and the time when the

pressure drops to 80% p_5. The reaction time is at a nominal value of 4.0 ms with the current experimental configuration [12]. An air-actuated valve, supplied by the High Pressure Equipment Company (HiP), is mounted in the center of the endwall to sample the post-shock reaction mixtures. The operation of the sampling valve is triggered by the endwall pressure signal with a delay of 4.0 ms (see Fig. 1), equal to the nominal reaction time. The opening and closing of the valve takes hundreds of milliseconds, withdrawing a sample of a relatively big quantity (equivalent to about 20 ml at 2 bar), to ensure sufficient sensitivity for trace PAH measurements. Due to the big sample volume, the average shock velocity, instead of the extrapolated value at the endwall, is used for the subsequent determination of T_5 and p_5. In this way, the real conditions encountered by the samples can be better represented. For most experiments, the shock velocity attenuation is within 2.5%, so the difference between the T_5s calculated based on the averaged and the extrapolated (local at the endwall) shock velocities is below 20 K, within the uncertainty specified above.

The sampled gas is transferred to the analytical system through SilcoTek tubes, which are heated at 250 °C to avoid condensation. The first GC (Agilent 7890) is equipped with a flame ionization detector (FID) connected to a DB-17-ms column for the measurements of heavy species. A thermal conductivity detector (TCD) is coupled to a Molsieve 5A column to monitor the absence of air. An external valve box which can regulate the temperature up to 320 °C is used for this GC to minimize the loss of heavy compounds due to condensation. An FID coupled to an HP Plot Q column is installed in the second GC (Thermo Trace GC Ultra), used for the measurements of small hydrocarbons, and a DSQ^{TM} (dual stage quadrupole) mass spectrometer is also connected to help the species identification. The connections in the analytical system and the operation parameters have been optimized in this work, bringing benefits from different aspects, including increased sensitivity of trace PAH species and better separation of PAH species that have similar retention time. For instance, the $C_{14}H_{10}$ isomers, phenanthrene and anthracene, which appear at 11.41 and 11.50 min, respectively, can be better separated and quantified now. PAH species up to four rings, with the peak concentration above 10^{-2} ppm level can be detected in the current experiments.

The identification of PAH species mainly depends on their retention time known through injections of standards. For species without available standards, the mass spectrometer provides molecular weights information, from which it is possible to infer the element composition, and it also suggests possible isomeric candidates. The addition of C_2 fuels introduces new species, such as a series of C_9 species that were negligible in our previous work on neat toluene pyrolysis [12]. Figure 2 shows the GC signals for the C_9 species. Indene and indane are identified according to their retention time. For other small peaks, their formulas are known from mass spectrometry, but their structures cannot be unambiguously identified, because some possible isomers have similar fragmentation patterns and standard mass spectra for some candidates are not available in the library. As presented in Fig. 2, these C_9H_8 species in toluene/acetylene pyrolysis are assigned as ethynyl-toluene and propynyl-benzene isomers, and the C_9H_{10} compounds in toluene/ethylene pyrolysis are taken as vinyl-toluene and propenyl-benzene isomers. In the later discussion, summed concentrations of C_9H_8 (excluding indene) and C_9H_{10} (excluding indane) are provided to compare with modeling results.

The quantification of species concentrations relies on calibrations for the FID response, and the procedures of the calibration experiments are detailed in [12,40]. Small hydrocarbons, except diacetylene (C_4H_2) and triacetylene (C_6H_2) are calibrated using standard mixtures with known compositions. The calibration of C_4H_2 and C_6H_2 is achieved in acetylene (C_2H_2) high temperature pyrolysis experiments based on the carbon atom conservation. Major PAH species up to three rings, including indene, indane, naphthalene, acenaphthalene, bibenzyl, biphenylmethane, fluorene, phenanthrene and anthracene, are calibrated in gas phase through the following procedures: i) known amounts of specific PAH compounds are dissolved in methanol to prepare the calibration solutions; ii) a small quantity (1–5 µl) of the solution is injected into a glass vessel (with a volume of 500 ml) using a GC syringe; the solution vaporizes immediately in the glass vessel, which is previously vacuumed and heated up at 150 °C; iii) the vessel is then filled with argon to a pressure of around 900 Torr, and the resulting gas mixture containing PAH standards stands for around 10–15 min to guarantee good homogeneity; iv) the gas mixture is injected into the GC system at least three times to check for consistency and the peak areas for the corresponding PAH standard are normalized by the injection pressure; v) the procedure is repeated at several standards mole fractions which cover the needed range for experiments, and the corresponding calibration factors are derived. Four-ring PAHs (pyrene and fluoranthene) cannot be steadily vaporized with the above approach. Therefore, their calibration factors are determined through an extrapolation from those of the two- and three- ring PAHs, namely, naphthalene and phenanthrene. The uncertainty in the concentration measurements is expected to be within 5% for directly calibrated small species, and 10%–15% for PAH species calibrated in gas phase, while the error in measured concentrations of four-ring PAH species may increase to 50%. Measurements presented in our previous publications [12,38,39] have proven the reliability and the good repeatability of the experimental set-up.

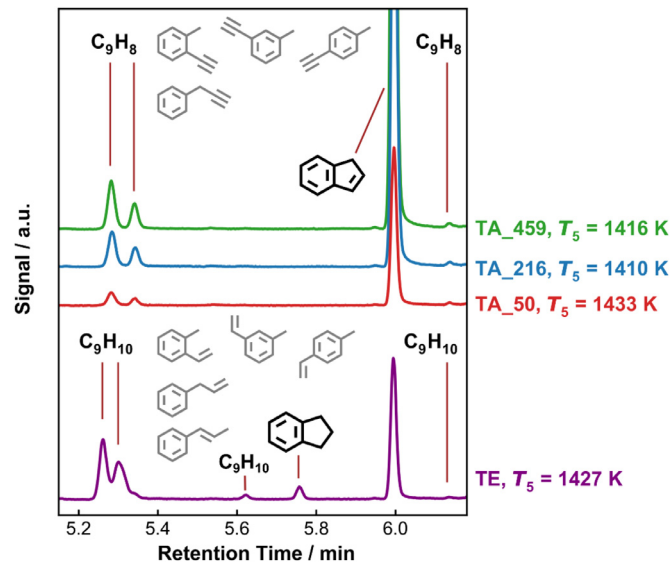

Fig. 2. GC signals for C_9 species detected in the toluene/C_2 pyrolysis experiments. The molecules in gray are possible candidates according to the mass spectra.

For the chemicals used in the experiments, toluene (with a purity of 99.8%) and PAH standards are purchased from Sigma-Aldrich, and the gases, including acetylene (>99.5%), ethylene (>99.5%), argon (>99.9999%) and helium (>99.995%), are supplied by Air Liquide. A 450B Matheson gas purifier with a 454 cartridge is connected to the acetylene bottle to remove possible acetone traces, and acetone is found below the detection limit of the GC system in all experiments. The experimental mixtures are prepared in a 136 L electropolished stainless steel cylinder which is previously evacuated to pressures below 10^{-5} mbar with a turbomolecular pump. To prepare an experimental mixture with a required composition, the fuel components are introduced into the

cylinder and the partial pressures are measured with a 0–10 Torr MKS Baratron pressure transducer (model 122BA). Argon is then added to a pressures of around 10 bar, monitored by a 0–10,000 Torr MKS Baratron pressure transducer (model 627D). Before the experiments, the gas mixture rests overnight to homogenize and the actual composition is analyzed with the GC, as listed in Table 1. The driven section is vacuumed with a turbomolecular pump till the pressure is below 10^{-5} torr before being filled with the experimental mixture. The carbon balance as a function of T_5 in each experimental set is presented in Fig. S1. The carbon balance keeps above 95% as T_5 is less than 1400 K, while deteriorating to 70−80% at higher temperatures. This is mainly due to the formation of heavy PAH species beyond our detection capabilities and soot particles. Besides, the carbon recovery improves when reducing the toluene contents in the experimental mixture, suggesting the important effects of aromatic species on the sooting tendency. The inner surface of the shock tube is cleaned every day to remove the carbon deposit. Each of the four experimental sets includes around 20 experiments, for which the nominal p_5 is 20 bar and T_5 ranges from 1100 K to 1650 K. The experimental results are provided in the *Supplementary Material*, including the post-shock conditions T_5 and p_5, the species concentrations as well as the endwall pressure histories up to 10 ms of individual experiments.

3. Kinetic modeling

Continuous efforts are made, based on our recent works towards constructing a predictive kinetic model for PAH formation from the pyrolysis of aromatic fuels. Previously, reaction sequences describing PAH speciation from toluene decomposition was developed and validated against the detailed measurements of toluene pyrolysis [12]. Later, benzyl related pathways were further tested with the experiments of C_8−C_{10} alkylbenzene pyrolysis [39], where the PAH formation is also controlled by benzyl chemistry. The C_2 sub-mechanism was updated in the discussion on the interactions between phenylacetylene and acetylene/ethylene [38]. In this work, particular attention is paid to the reactions between C_2 and toluene fuel radicals. Reactions updated in the current work are listed in Table S1 in the *Supplementary Material* together with the adopted rate coefficients.

The reaction system of benzyl (C_7H_7)+acetylene (C_2H_2) was studied in previous theoretical works [17,18], since it is a potential indene source under combustion-relevant conditions. Vereecken and Peeters [18] performed RRKM/ME calculations based on a density functional potential energy surface (PES). The formation of indene (C_9H_8)+H was identified as the predominant channel and a rate coefficient at its high-pressure limit was reported [18]. Later, Mebel et al. [17] revisited the PES of C_7H_7 + C_2H_2 reactions at G3(MP2, CC) level of theory and derived pressure-dependent rate coefficients of involved reactions over the temperature range of 500−2500 K. Only the formation of two pairs of bimolecular products, indene (C_9H_8)+H and 3-phenylpropyne ($C_6H_5CH_2C{\equiv}CH$)+H, has kinetic significance under the currently concerned high-pressure conditions. Besides, $C_6H_5CH_2C{\equiv}CH$ can also convert to C_9H_8 through H-assisted isomerization. The reactions between phenyl (C_6H_5) and C_3H_4 (allene and propyne) also result in the formation of $C_6H_5CH_2C{\equiv}CH$, and these reactions were theoretically explored in the same work by Mebel et al. [17]. All mentioned relevant reactions with their theoretically-determined rate coefficients [17] are incorporated in the current model. Reactions between benzyl (C_7H_7) and ethylene (C_2H_4) have not been addressed through theoretical approaches in literature to the best of our knowledge. Herein, we consider that they proceed in a similar manner with C_7H_7 + C_2H_2 reactions, leading to the formation of the cyclic species indane (C_9H_{10}) and the single-chain aromatic 3-phenyl-1-propene ($C_6H_5CH_2CH{=}CH_2$). The rate coefficient of C_7H_7+C_2H_2 = C_9H_8+H from [18] is assigned to the C_9H_{10} formation channel, and the rate coefficient of C_7H_7+C_2H_4 = $C_6H_5CH_2CH{=}CH_2$+H is determined through an analogy to the reaction CH_3+C_2H_4 = C_3H_6+H. In particular, the reaction rate constant of the C_7H_7+C_2H_2 reaction in [18] (used for the C_7H_7+C_2H_4 reaction in the current model) is about 9–10 times lower in the temperature range 1200–1550 K compared to the one calculated by Mebel et al. [17] at 10 atm. The choice of a lower reaction rate constant for the C_7H_7+C_2H_4 reaction is backed up by experimental evidences as discussed later in Section 4.2. Nevertheless, future theoretical works are highly demanded to map out the reactions on the C_7H_7 + C_2H_4 surface and to derive accurate kinetic parameters. Regarding the consumption of C_9H_{10}, besides the H_2 elimination forming indene (C_9H_8), ring-opening processes leading to o-vinyl-toluene ($CH_3C_6H_4CH{=}CH_2$) and 3-phenyl-1-propene ($C_6H_5CH_2CH{=}CH_2$) are also taken into account. Rate coefficients for these ring-opening reactions are evaluated through analogies to the isomerization of cyclopentene to 1,3-pentadiene ($CH_3CH{=}CHCH{=}CH_2$) and 1,4-pentadiene ($CH_2{=}CHCH_2CH{=}CH_2$) [41], respectively. Methyl-phenyl ($CH_3C_6H_4$) is considered as a minor fuel radical of toluene, in comparison to its resonantly stabilized counterpart C_7H_7. The detection of C_9 species with the structure of $CH_3C_6H_4C_2H_x$ in the current experiments, however, suggests the participation of $CH_3C_6H_4$ in relevant formation reactions. Addition-elimination reactions between $CH_3C_6H_4$ and C_2H_x forming $CH_3C_6H_4C_2H_x$+H are considered in the current model, and the rate coefficients of the analogous phenyl + C_2H_x reactions are used in corresponding cases. The consumption of $CH_3C_6H_4C_2H_x$ is considered to proceed through a similar scheme to that of toluene. The current model includes reactions between indenyl (C_9H_7) and acetylene producing ethynyl-indene ($C_9H_7C_2H$) and methyl naphthalene radical ($C_{10}H_7CH_2$), for which the rate coefficient originate from a recent kinetic model for indene pyrolysis [42].

As mentioned in the experimental section, the $C_{14}H_{10}$ isomers, phenanthrene ($PC_{14}H_{10}$) and anthracene ($AC_{14}H_{10}$), can be well quantified in the current experiments. $PC_{14}H_{10}$ was found as a major three-ring PAH species, and $AC_{14}H_{10}$ was also measured of non-negligible amounts. The formation of three-ring PAHs from benzyl recombination was theoretically explored by Sinha and Raj [16], and $PC_{14}H_{10}$ was identified as the major product. Relevant stepwise isomerization and ring-closure reactions were already included in our kinetic model [12]. These pathways help in improving the model prediction for $PC_{14}H_{10}$ concentrations, however, cannot form sufficient $AC_{14}H_{10}$ to match the experimental measurements. The isomerization between $PC_{14}H_{10}$ and $AC_{14}H_{10}$, with the rate coefficients reported by Colket and Seery [43], is also included in the model, but this reaction results in a net production of $PC_{14}H_{10}$ over the investigated temperature range. Discussion on the formation of $AC_{14}H_{10}$ is relatively limited in literature, compared to that of $PC_{14}H_{10}$. In the latest CRECK model [44] describing PAH formation, two lumped reactions, C_7H_7+$CH_3C_6H_4$ = $C_{14}H_{10}$+2H+H_2 and $CH_3C_6H_4$+$CH_3C_6H_4$ = $C_{14}H_{10}$+2H+H_2, are included in the mechanism to interpret the formation of the lumped $C_{14}H_{10}$ species. As shown in Scheme 1, the recombination steps result in two different $C_{14}H_{14}$ molecules, 2-methyldiphenylmethane and 2,2′-dimethylbiphenyl, separately. Similar to the case of benzyl self-recombination, the subsequent dehydrogenation and isomerization processes may lead to both $AC_{14}H_{10}$ and $PC_{14}H_{10}$. In the current model, $AC_{14}H_{10}$ and $PC_{14}H_{10}$ are assigned as the products of the lumped reactions starting from $CH_3C_6H_4$+C_7H_7 and $CH_3C_6H_4$+$CH_3C_6H_4$, respectively. Such an assumption is based on the structural features of the corresponding $C_{14}H_{14}$ molecules, as can be noted from Scheme 1.

Since the kinetic model development in our works [12,38,39] is based on the latest version of CRECK model [44], the

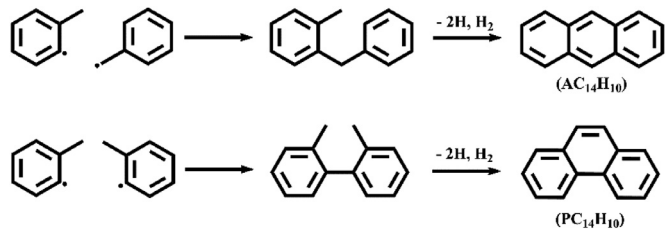

Scheme 1. Potential pathways starting from toluene fuel radicals leading to $C_{14}H_{10}$ isomers.

thermochemical data used in our model are mostly from the CRECK model [44]. For species that are missing from the CRECK model [44], such as indane (C_9H_{10}), indanyl (C_9H_9) and anthracene ($AC_{14}H_{10}$), corresponding thermochemical parameters come from the database of Burcat [45]. The kinetic model, including the reaction mechanism and the specie thermochemical data, is provided in the *Supplementary Material*. Simulations in the present work were performed with the homogenous reactor model of the software COSILAB [46] using two different methods: a nominal reaction time of 4.0 ms and a constant pressure of 20 bar are used in the first method. The constant pressure assumption in simulating the speciation sampled from single-pulse shock tube experiments was well justified in previous publications [47,48]. The other method is to employ the measured pressure profiles up to 10.0 ms to simulate each shock operation and then gather the final species concentrations that no longer vary with the time. This takes account of the reactions that may occur in the quenching period [41,49,50], particularly those involving resonantly stabilized radicals such as benzyl. Simulated results for specific species with the two different modes will be compared in the following discussion.

4. Results and discussion

Predictive performances of the kinetic model are examined with species concentration measurements, in particular, for important aromatic intermediates and products. For comparison purpose, the kinetic model proposed in the recent work [37] is also used to simulate the speciation measurements obtained in the current work. Experimental and modeling species concentration profiles for individual species in all four investigated sets are shown in Figs. S2–S5 in the *Supplementary Material*. The current model can better capture the fuel decomposition reactivity, and more importantly, the speciation of the aromatic products that is targeted in this work. Overall, the major PAH species, with the peak concentrations above 1 ppm, include indene, naphthalene, acenaphthalene, bibenzyl, fluorene and phenanthrene, and the relative abundance of these PAHs are altered by the fuel composition. The speciation of most PAH species occurs in the temperature regime of 1400–1600 K, though for specific species such as indene, this window shifts to lower temperatures when adding C_2 fuels. In the following discussion, experimental observations and analyses with the validated kinetic model are combined to reveal the influences of the C_2H_4 and C_2H_2 addition on the speciation from toluene pyrolysis. Attention is paid to compare the effects brought by the separate addition of C_2H_2 and C_2H_4, and to illustrate the variation trends of specific species concentrations when different amounts of C_2H_2 are present in the fuel mixtures.

4.1. Fuel decomposition and mono-aromatic ring intermediates

Figure 3 displays the fuel concentrations as a function of the post-shock temperature T_5 in separate cases of toluene/C_2H_2 (or C_2H_4) pyrolysis. The kinetic model satisfactorily predicts the measured fuel conversion profiles in individual studied cases. To

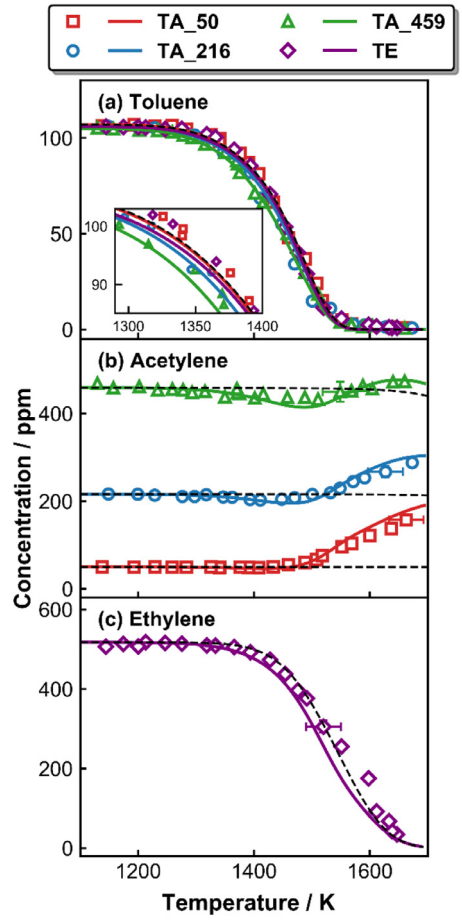

Fig. 3. Measured (symbols) and simulated (lines) fuel concentrations as a function of the post-shock temperature T_5 in toluene/acetylene (ethylene) pyrolysis. The dark dashed lines are simulated fuel decomposition profiles of (a) neat toluene (106 ppm in argon), (b) neat acetylene (50, 216 and 459 ppm in argon) and (c) neat ethylene (518 ppm in argon). The inset of (a) shows toluene concentrations over the temperature range of 1300−1400 K.

better illustrate the mutual effects between the binary fuel components, simulated fuel decomposition profiles of neat toluene, neat C_2H_2 and neat C_2H_4 are also shown in Fig. 3 as a reference. Given the almost identical contents of toluene in separate cases and an estimated uncertainty of ±30 K in the calculated T_5, the effects of added C_2 fuels on toluene decomposition reactivity are not noticeable on the largely overlapped toluene concentration profiles. Thus, toluene concentrations over 1300−1400 K, where the consumption of toluene just begins, are zoomed in and shown in the inset of Fig. 3(a). Experimental and modeling results consistently suggest that the increased C_2H_2 contents in the binary mixtures promote toluene decomposition. The C_2H_4 addition also enhances toluene decomposition reactivity, but to a lesser extent than C_2H_2. According to the rate-of-production (ROP) analyses for toluene consumption, in all studied cases, toluene decomposition is initiated via the loss of the benzylic hydrogen ($C_7H_8(+M) = C_7H_7+H(+M)$), while at higher temperatures, toluene is consumed mainly through the hydrogen abstraction by H atom forming benzyl (C_7H_7) ($C_7H_8 + H = C_7H_7+H_2$). Simulated H atom concentrations as a function of T_5 in individual cases are shown in Fig. 4(a). Among all the cases of toluene/C_2 pyrolysis, the toluene decomposition reactivity follows the same order of the H atom concentrations below 1450 K. The slight decrease and the subsequent rise at elevated temperatures in C_2H_2 concentrations (see Fig. 3(b)) come from an overall effect of the reactions between

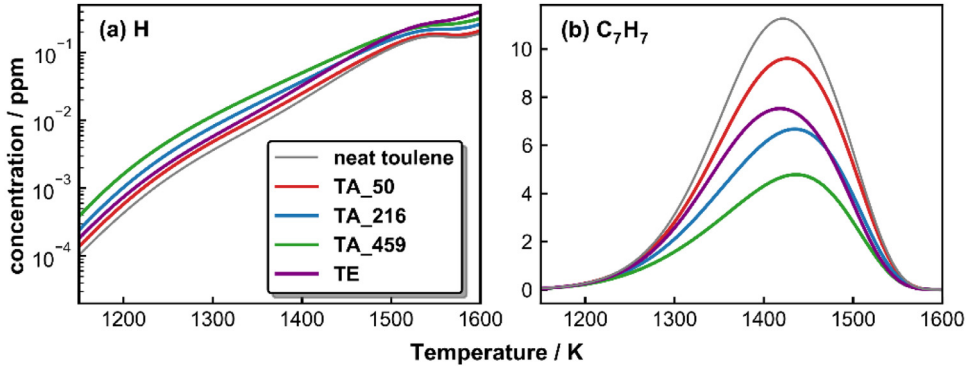

Fig. 4. Simulated H atom and benzyl radical (C_7H_7) concentrations in the pyrolysis of neat toluene (106 ppm in argon) and toluene/acetylene (ethylene) binary mixtures.

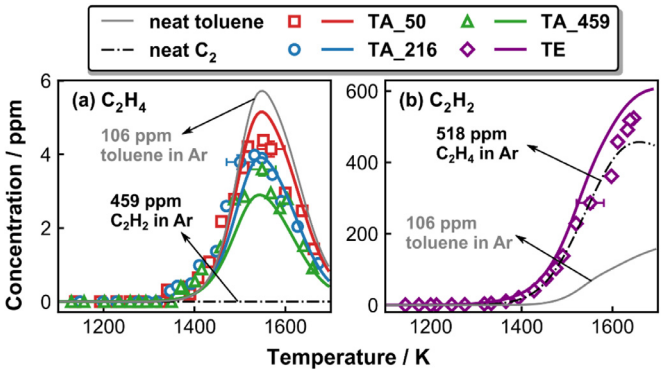

Fig. 5. Measured (symbols) and simulated (lines) concentration profiles of (a) ethylene in toluene/acetylene pyrolysis and (b) acetylene in toluene/ethylene pyrolysis. Simulated concentrations in neat toluene (106 ppm in argon) and neat acetylene/ethylene pyrolysis are also shown as a reference.

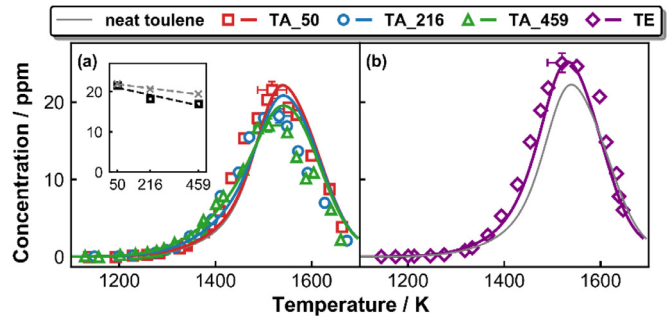

Fig. 6. Experimental (symbols) and modeling (solid lines) benzene (C_6H_6) concentrations as a function of the post-shock temperature T_5 in (a) toluene/C_2H_2 pyrolysis and (b) toluene/C_2H_4 pyrolysis. The inset in (a) plots the measured (dark open square) and simulated (gray cross) peak C_6H_6 concentrations against the initial C_2H_2 contents; linear regressions (the dashed lines) of the data points are shown as a visual guide. The simulated C_6H_6 concentration profile in neat toluene pyrolysis (the gray solid line) is shown as a reference.

C_2H_2 and toluene related radicals, the C_2H_2 thermal decomposition and the C_2H_2 formation from toluene consumption. Such phenomena can be well reproduced by the current kinetic model in all three cases of binary toluene/C_2H_2 mixtures pyrolysis. Moreover, compared to the case of neat C_2H_2 pyrolysis at identical initial concentrations, C_2H_2 starts to decompose at lower temperatures in the binary mixture pyrolysis, and such effects are more obvious when raising the initial C_2H_2 contents. The synergistic effects between toluene and C_2H_2 is also presented in the recent study by Li et al. [37], and the authors attributed the enhanced fuel decomposition reactivity to the reaction $C_7H_7+C_2H_2 = C_9H_8+H$. This process consumes C_2H_2 at relatively low temperatures, and produces H atoms which can facilitate the hydrogen abstractions from both toluene and C_2H_2. The presence of toluene also promotes the decomposition of C_2H_4, but to a smaller extent in comparison to that of C_2H_2. The synergistic effects observed in toluene/C_2H_4 pyrolysis arise from a similar mechanism, mainly through reactions between benzyl and C_2H_4. Detailed discussion on the interaction between the binary fuel components and the directly affected speciation behaviors will be presented in Section 4.2.

C_2H_2 and C_2H_4 have distinct decomposition reactivity, and in reality, they also exhibit different speciation behaviors as intermediates in the currently studied cases. Concentration profiles of C_2H_4 in toluene/C_2H_2 pyrolysis and C_2H_2 in toluene/C_2H_4 pyrolysis are presented in Fig. 5. The simulated concentration distributions in neat toluene, acetylene and ethylene pyrolysis are also shown for comparison. It is seen that the pyrolysis of C_2H_2 does not contribute to the formation of C_2H_4, and instead, the addition of C_2H_2 reduces the C_2H_4 production from toluene consumption (see Fig. 5(a)). As will be detailed later, the added C_2H_2 alters the consumption pathway of toluene and its radicals. One of the consequences is that the formation of C_2H_5, the major precursor of C_2H_4, is inhibited. C_2H_5 mainly comes from the dehydrogenation of C_2H_6 following the CH_3 recombination, and CH_3 in the reaction system originates from the CH_3 side chain of toluene molecule. Differently, in toluene/C_2H_4 pyrolysis, all C_2H_4 is essentially converted to C_2H_2 (see Fig. 5(b)). This observation indicates that the toluene-C_2H_2 chemistry also plays an important role in toluene/C_2H_4 pyrolysis.

Benzene (C_6H_6) is one of the major products of toluene/C_2 binary mixtures pyrolysis, and the experimental and modeling C_6H_6 concentrations, as a function of T_5, are shown in Fig. 6. Simulated C_6H_6 speciation profile in neat toluene (106 ppm in argon) is also provided as a reference. The addition of both C_2H_2 and C_2H_4 lowers the C_6H_6 formation temperature. This is because the increased H atom concentrations (see Fig. 4(a)) facilitate C_6H_6 formation through the ipso-substitution reaction $C_7H_8+H = C_6H_6+CH_3$. However, the two C_2 fuels have opposite effects on the peak concentrations of C_6H_6: the added C_2H_2 slightly reduces C_6H_6 peak concentrations, and such effects are more pronounced when increasing the initial C_2H_2 concentration. Differently, the presence of C_2H_4 results in an increment in C_6H_6 peak concentrations, in comparison to neat toluene pyrolysis. The current model can correctly reproduce the early C_6H_6 formation brought by added C_2, and accurately capture the variation trend of C_6H_6 peak concentrations when altering the initial fuel compositions.

To better understand the different influences on C_6H_6 peak concentrations of C_2H_2 and C_2H_4 addition, sensitivity analyses for C_6H_6 are performed at 1500 K, where the C_6H_6 concentrations are approaching their maxima. The analyzed sensitivity spectra are

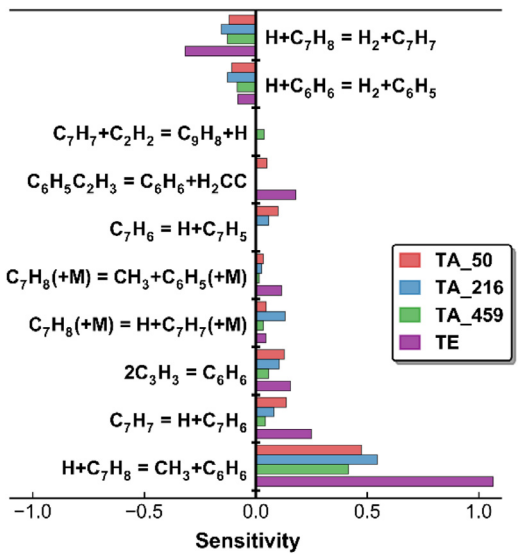

Fig. 7. Sensitivity analyses for C_6H_6 at T_5 = 1500 K in toluene/C_2 binary mixtures pyrolysis.

presented in Fig. 7. In all studied cases of toluene/C_2 pyrolysis, the predominant C_6H_6 formation reaction, H + C_7H_8 = CH_3+C_6H_6, has the highest positive sensitivity coefficient promoting C_6H_6 production, while its competing channel, the hydrogen abstraction reaction, H + C_7H_8 = H_2+C_7H_7, has remarkable inhibiting effects. Apart from the reactions directly producing C_6H_6, reactions that generate H atoms also have positive coefficients on the sensitivity spectra. As mentioned above, the reaction C_7H_7+C_2H_2 = C_9H_8+H is an important source of H atoms, which improves the fuel decomposition reactivity in toluene/C_2H_2 pyrolysis. However, this reaction is not among the most sensitive reactions for C_6H_6 formation. The reason lies in the fact that at elevated temperatures such as the analyzed 1500 K, H atoms are predominantly contributed by the C_7H_7 decomposition through $C_7H_7 \rightarrow C_7H_6 \rightarrow C_7H_5$, instead of the addition-elimination reaction C_7H_7+C_2H_2 = C_9H_8+H. However, the level of C_7H_7 is significantly reduced (see Fig. 4(b)) due to its recombination reaction with C_2H_2 forming indene+H. The propargyl (C_3H_3) formation from C_7H_5 decomposition (C_7H_5 = C_3H_3+C_4H_2) is also impeded, and therefore the sensitivity of the C_3H_3 self-recombination forming C_6H_6 decreases when increasing the C_2H_2 contents in the fuel mixtures. Concerning the toluene/C_2H_4 pyrolysis, a remarkable amount of H atoms is produced at elevated temperatures (see Fig. 4(a)) from C_2H_4 consumption. Besides, the inhibition on C_7H_7 decomposition is not as pronounced as in the cases of toluene/C_2H_2 pyrolysis, because of the lower reactivity of the benzyl+C_2H_4 reaction, as will be discussed in Section 4.2. Furthermore, the styrene ($C_6H_5C_2H_3$) decomposition reaction, $C_6H_5C_2H_3$ = C_6H_6+H_2CC, appears as an alternative C_6H_6 producing channel in toluene/C_2H_4 pyrolysis. These multiple factors explain the increased C_6H_6 peak concentration in toluene/C_2H_4 pyrolysis.

Figure 8 displays the experimental and modeling concentration profiles of C_8 mono-aromatic hydrocarbon (MAH) species, including ethylbenzene ($C_6H_5C_2H_5$), styrene ($C_6H_5C_2H_3$) and phenylacetylene ($C_6H_5C_2H$), in the pyrolysis of toluene/C_2 binary mixtures. For all three C_8 MAHs, the current kinetic model can well capture the variation trends of their peak concentrations when altering the initial fuel compositions. The added C_2H_2 and C_2H_4 reduces the formation of $C_6H_5C_2H_5$, and C_2H_2 exhibits more pronounced effects if the same amount of C_2H_2 and C_2H_4 are added. Such inhibiting effects arise from the fact that a part of C_7H_7 reacts with the added C_2H_2 or C_2H_4, so that the carbon flux into $C_6H_5C_2H_5$ through C_7H_7+CH_3 recombination is decreased. C_2H_2 and C_2H_4 have opposite effects on the formation of $C_6H_5C_2H_3$. A clear decreasing trend is noted in the peak $C_6H_5C_2H_3$ concentrations when increasing the initial C_2H_2 contents, while the $C_6H_5C_2H_3$ production from toluene pyrolysis is doubled by the addition of C_2H_4. Such differences can be explained by the varied dominant $C_6H_5C_2H_3$ formation pathways: in neat toluene and toluene/C_2H_2 mixture pyrolysis, $C_6H_5C_2H_3$ is mainly produced from the consumption of $C_6H_5C_2H_5$, while the reaction C_6H_5+C_2H_4 = $C_6H_5C_2H_3$+H governs the $C_6H_5C_2H_3$ formation when C_2H_4 is introduced. The speciation temperature windows for the above-mentioned $C_6H_5C_2H_5$ and $C_6H_5C_2H_3$ are not significantly changed by the addition of C_2 hydrocarbons. However, the formation of $C_6H_5C_2H$ shifts towards lower temperatures when C_2H_2 or C_2H_4 is present in the fuel mixtures. Meanwhile, the peak concentrations increase, particularly when C_2H_2 is added to toluene pyrolysis. The formation of $C_6H_5C_2H$ relies on the reactions between phenyl (C_6H_5) and C_2H_2, and C_6H_5 mainly comes from toluene unimolecular decomposition (C_7H_8(+M) = C_6H_5+CH_3(+M)). In neat toluene pyrolysis, the production of $C_6H_5C_2H$ is limited by the level of C_2H_2, which is largely produced only at elevated temperatures above 1450 K. This explains how C_2H_2, either already existing in fuel mixtures or produced from C_2H_4 decomposition, enhances the production of $C_6H_5C_2H$ at relatively low temperatures.

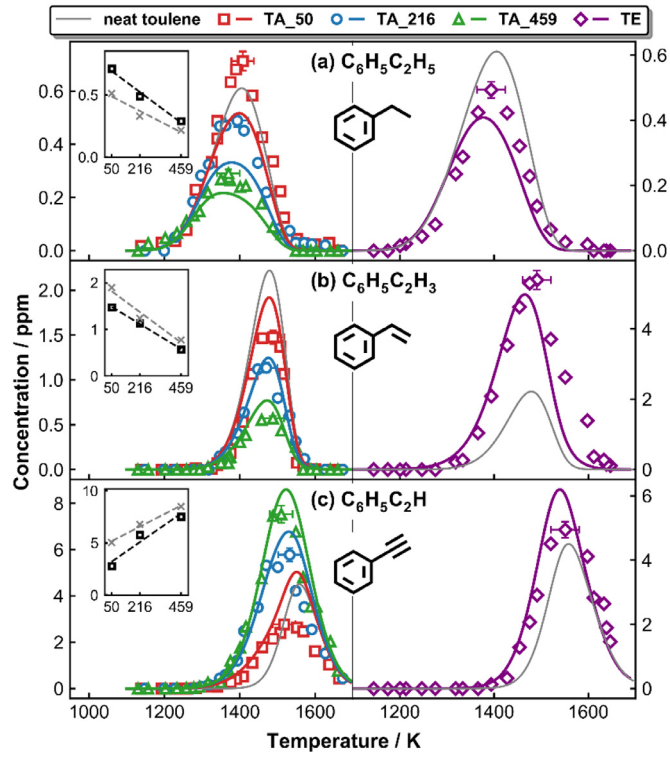

Fig. 8. Experimental (symbols) and modeling (solid lines) concentrations of C_8 MAH species as a function of the post-shock temperature T_5. The left panel: toluene/C_2H_2 pyrolysis; the upper left insets plot the measured (dark open square) and simulated (gray cross) peak concentrations of separate species against the initial C_2H_2 contents; linear regressions (the dashed lines) of the data points are shown as a visual guide. The right panel: toluene/C_2H_4 pyrolysis. The simulated species concentration profiles in neat toluene pyrolysis (the gray solid lines) are shown as a reference.

4.2. Intermediates and products from toluene radicals-C_2 interactions

As already mentioned above, the synergistic effects on fuel decomposition reactivity in toluene/C_2 binary mixture pyrolysis

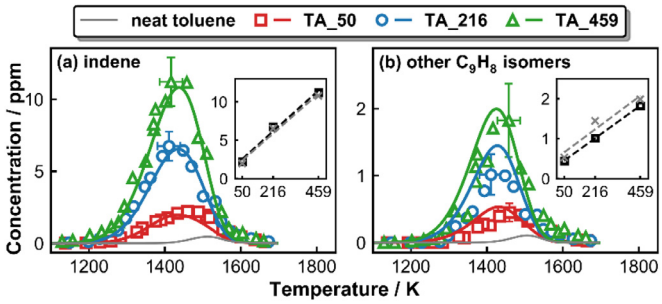

Fig. 9. Experimental (symbols) and modeling (solid lines) concentrations of C_9H_8 species as a function of the post-shock temperature T_5 in toluene/acetylene pyrolysis. The upper right insets plot the measured (dark open square) and simulated (gray cross) peak concentrations of separate species against the initial C_2H_2 contents; linear regressions (the dashed lines) of the data points are shown as a visual guide. Simulated concentration profiles in neat toluene pyrolysis (the gray solid lines) are shown as a reference.

derive from the interactions between toluene radicals and the C_2 fuels. A direct proof is offered by the observation of abundant C_9 species. In toluene/C_2H_2 pyrolysis experiments, indene is identified as the dominant C_9H_8 species, and minor amounts of other C_9H_8 isomers, propynyl-benzene ($C_6H_5C_3H_3$) and ethynyl-toluene ($CH_3C_6H_4C_2H$) species, are also detected (see Fig. 2). Figure 9 presents the experimental and modeling concentration profiles for indene and the sum of other C_9H_8 isomers in toluene/C_2H_2 pyrolysis, and the variation trends of the peak concentrations against the initial C_2H_2 concentrations are also shown. By adopting the rate coefficient reported by Mebel et al. [17], the current kinetic model can precisely predict indene concentrations over the entire temperature range in all three toluene/C_2H_2 experimental sets with different initial C_2H_2 concentrations. The minor C_9H_8 species have a similar speciation temperature window to that of indene, and they form via the addition of C_7H_7 or $CH_3C_6H_4$ to the triple bond of C_2H_2. For both indene and other minor C_9H_8 isomers, their peak concentrations almost linearly increase with the quantity of C_2H_2 added to toluene pyrolysis, and such a trend can be well predicted by the kinetic model. Indene speciation profile in neat toluene (106 ppm in argon) pyrolysis is shown as a reference: it starts to form slightly above 1400 K, and reaches a peak concentration below 1 ppm at around 1500 K. The presence of C_2H_2 lowers the onset temperature to about 1200 K, and remarkably facilitates indene production: Even by adding only 50 ppm C_2H_2, the peak concentration of indene reaches over 2 ppm. This suggests the role of the reaction $C_7H_7+C_2H_2 = C_9H_8+H$ as an efficient pathway producing indene.

The indene concentration profile in toluene/C_2H_4 pyrolysis is shown in Fig. 10, which also displays the concentration profiles of C_9H_{10} species, including indane and other isomers, namely, propenyl-benzene ($C_6H_5C_3H_5$) and vinyl-toluene ($CH_3C_6H_4C_2H_3$) species (see Fig. 2). C_2H_4 in the fuel mixture can also lower the indene speciation temperature and enhance the indene production, but to a lesser extent in comparison to C_2H_2 if the same amounts of C_2H_2 and C_2H_4 are concerned. With over 500 ppm C_2H_4 added to toluene pyrolysis, the resulting peak indene concentration is about 4 ppm, falling between those in TA_50 and TA_216 pyrolysis (see Fig. 9). Indane is expected to be abundant in toluene/C_2H_4 pyrolysis, as its production from the interaction between C_7H_7 and C_2H_4 through $C_7H_7+C_2H_4 = C_9H_{10}+H$ is thought to be efficient. However, only a trace quantity (10^{-1} ppm level) of indane is measured in toluene/C_2H_4 pyrolysis. The limited production and the quick consumption of indane together account for the low concentrations of indane observed in toluene/C_2H_4 pyrolysis. More specifically, the indane formation from $C_7H_7+C_2H_4$ proceeds at a slower rate than the $C_7H_7+C_2H_2$ reaction producing indene; and indane rapidly decomposes to indene or isomerizes through ring-opening processes under the investigated conditions. At relatively low temperatures, the decomposition of indane governs the indene formation; while at elevated temperatures, the efficient indene formation channel, $C_7H_7+C_2H_2 = C_9H_8+H$, becomes dominant, as considerable C_2H_2 is formed from C_2H_4 decomposition. As mentioned in the modeling section, the rate coefficient of the reaction $C_7H_7+C_2H_4$ = indane+H is assessed through an analogy to the reaction $C_7H_7+C_2H_2$ = indene+H reported in [18]. This practice potentially introduces uncertainties in the indane speciation kinetics, though the current model satisfactorily captures the measurements of C_9 species in toluene/C_2H_4 pyrolysis. Future theoretical works on the $C_7H_7+C_2H_4$ reaction system and how indane further dehydrogenates to form indene are highly necessary. Compared to indene and indane, the monocyclic C_9H_{10} isomers (see Fig. 10(c)) have significant contents in toluene/C_2H_4 pyrolysis. Allylbenzene ($C_6H_5C_3H_5$–1), 1-propenyl-benzene ($C_6H_5C_3H_5$–2) and lumped o-, m- and p- vinyl toluene isomers ($CH_3C_6H_4C_2H_3$) are included in the current kinetic model. Simulated concentration profiles of individual above-mentioned C_9H_{10} isomers are presented in Fig. S6 in the *Supplementary Material*. According to the model predictions, both $C_6H_5C_3H_5$–1 and $CH_3C_6H_5C_2H_3$ both have peak concentrations of about 1 ppm; the former peaks at around 1400 K while the later reaches its maximum at around 1500 K. The consumption of these C_9H_{10} isomers partly contributes the formation of indene through dehydrogenation and ring-closure steps.

It has been discussed in our previous work [12] that the benzyl (C_7H_7) chemistry controls the speciation, particularly for PAH species, in toluene pyrolysis. To explore the influences of the added C_2 fuels on C_7H_7 consumption, ROP analyses of C_7H_7 are performed at 1400 K, where abundant C_7H_7 exists in the toluene/C_2 pyrolysis reaction systems (see Fig. 4(b)). According to the results in Fig. 11, the fate of C_7H_7 is very sensitive to the initial fuel composition. C_7H_7 either decomposes, or reacts with other species, including the C_2 fuels, CH_3 and C_7H_7 itself. The contributions of reactions involving C_2 fuels increase notably with the initial C_2 concentrations. Thus, other competing pathways are inhibited, among

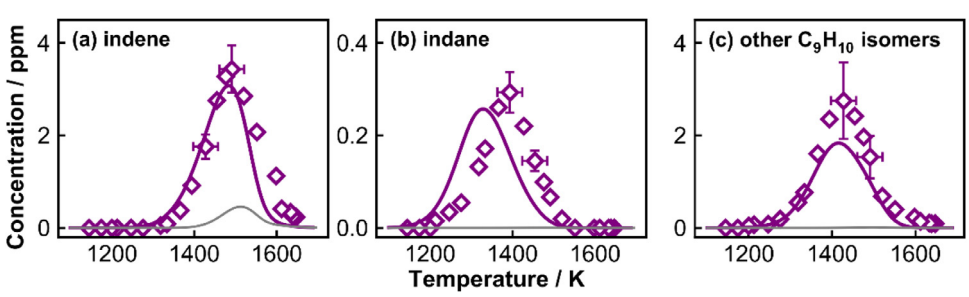

Fig. 10. Experimental (symbols) and modeling (solid lines) concentrations of C_9 species as a function of the post-shock temperature T_5 in toluene/ethylene pyrolysis. Simulated concentration profiles in neat toluene pyrolysis (the gray solid lines) are shown as a reference.

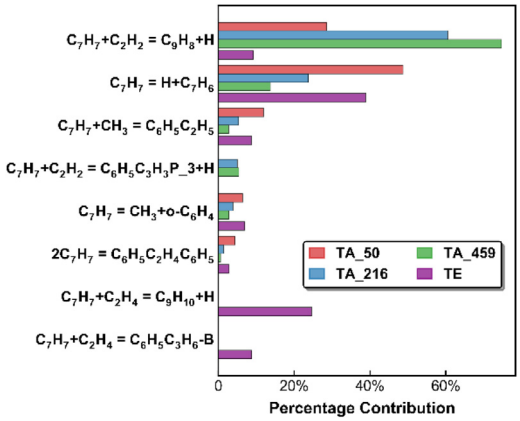

Fig. 11. ROP-analyzed percentage contributions to benzyl consumption in the pyrolysis of toluene/C_2 binary mixtures at 1400 K.

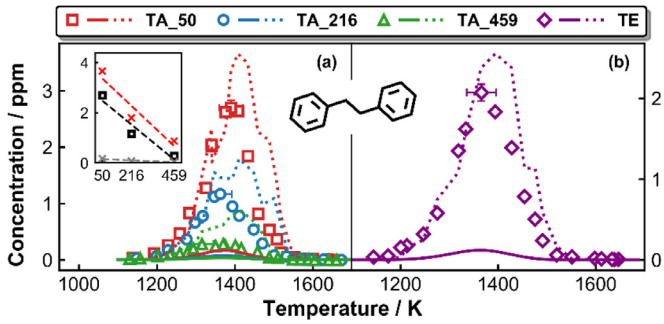

Fig. 12. Bibenzyl ($C_6H_5C_2H_4C_6H_5$) concentrations as a function of the post-shock temperature T_5 in (a) toluene/C_2H_2 pyrolysis and (b) toluene/C_2H_4 pyrolysis. Symbols: measurements; solid lines: simulations with a constant pressure of 20 bar within a reaction time of 4.0 ms; dotted lines: simulations with measured pressure histories up to 10 ms. The upper left inset in the left panel plot the measured (dark open square) and simulated (constant pressure assumption: gray cross; with measured pressure histories: red cross) peak $C_6H_5C_2H_4C_6H_5$ concentrations against the initial C_2H_2 contents; the linear regressions (the dashed lines) of the data points are shown as a visual guide. (For interpretation of the references to color in this figure legend, the reader is referred to the web version of this article.)

which the C_7H_7+CH_3 recombination the C_7H_7 self-recombination lead to ethylbenzene ($C_6H_5C_2H_5$) and bibenzyl ($C_6H_5C_2H_4C_6H_5$), respectively.

As discussed above, when adding C_2 fuels to toluene pyrolysis, the decrease in $C_6H_5C_2H_5$ peak concentrations is due to the reduced $C_6H_5C_2H_5$ formation through C_7H_7+CH_3. The production of $C_6H_5C_2H_4C_6H_5$, which comes almost exclusively from C_7H_7 self-recombination, is influenced to a greater extent. $C_6H_5C_2H_4C_6H_5$ was measured to be the most abundant PAH species in neat toluene pyrolysis [12], however, only 10^{-1} ppm level of $C_6H_5C_2H_4C_6H_5$ is detected in TA_459 pyrolysis. Figure 12 exhibits the experimental $C_6H_5C_2H_4C_6H_5$ concentrations that evolve with the temperature in toluene/C_2 pyrolysis. A sharp decline shows in peak concentrations of $C_6H_5C_2H_4C_6H_5$ when raising the initial C_2H_2 contents, and by adding over 500 ppm C_2H_4, the $C_6H_5C_2H_4C_6H_5$ peak concentration falls between those in TA_50 and TA_216 pyrolysis. Simulations with two different approaches are presented: using the constant pressure of 20 bar within the nominal reaction time of 4.0 ms and using the measured pressure histories up to 10.0 ms. The resulting $C_6H_5C_2H_4C_6H_5$ concentrations differ significantly, and only with the second method can the $C_6H_5C_2H_4C_6H_5$ concentrations be satisfactorily predicted.

It was addressed in our previous works [12,38,39] that reactions involving the resonantly stabilized benzyl radical can carry on during the post-shock quenching. So the simulated results are remarkably impacted by the adopted methods. Time-dependent concentrations of selected species in TA_459 and TE pyrolysis at T_5 around 1420 K are shown in Fig. 13, and those in TA_50 and TA_216 pyrolysis are provided in Fig. S7 in the *Supplementary Material*. It is seen that C_7H_7 survives the shock-heated period, still having relatively high concentrations (a few ppm) by the end of the reaction duration of 4.0 ms, and its consumption continues during the quenching period. This gives rise to that the majority of $C_6H_5C_2H_4C_6H_5$ is actually formed during the post-shock cooling. Ethylbenzene ($C_6H_5C_2H_5$) is also partly formed during the quenching, via the C_7H_7 + CH_3 recombination, as mentioned above. Reactions involving CH_3 may also lead to species formation during the quenching period, as pointed out by Manion et al. [49]. 1-methylindene ($C_9H_7CH_3$) is another species whose formation spans over the post-shock quenching, since it mainly forms through the recombination between CH_3 and the resonantly-stabilized indenyl (C_9H_7) radical. Nevertheless, for most species, the formation is completed before the arrival of the rarefaction waves, and their concentrations no longer change with the time afterwards. Therefore, the measured concentrations can be well reproduced by simulations over a reaction time of 4.0 ms based on the constant pressure assumption. Simulations for all species concentration profiles using the two different approaches are presented and compared in Figs. S2–S5 in the *Supplementary Material*.

4.3. Influences of C_2 addition on the speciation of two to four ring PAH species

One major purpose of this work is to illustrate the impacts of C_2 fuels on PAH speciation in toluene pyrolysis. Apart from the above discussed indene and bibenzyl, which are directly influenced by the C_2 addition, concentrations of numerous two- to four-ring PAH species are measured in each experimental set. Figure 14 presents the concentration profiles of C_{10} PAH species, including naphthalene ($C_{10}H_8$), benzofulvene ($C_9H_6CH_2$) and 1-methylindene ($C_9H_7CH_3$). Overall, the presence of C_2 fuels enhances the formation of the C_{10} PAHs, and the model can satisfactorily capture such trends though it "under-estimates" $C_9H_7CH_3$ concentrations. This is because a large portion of $C_9H_7CH_3$ is formed during the reaction quenching, as mentioned above. By using the measured pressure profiles, predicted $C_9H_7CH_3$ concentrations are largely enhanced (see Figs. S2–S5). $C_{10}H_8$ is one of the dominant PAH species produced from toluene pyrolysis. By taking the simulated $C_{10}H_8$ concentration profile in neat toluene pyrolysis as a reference, extra C_2H_2 and C_2H_4 both facilitate $C_{10}H_8$ formation, and the effects of C_2H_2 are more evident if the same amounts of C_2H_2 and C_2H_4 are concerned. Reaction pathways leading to $C_{10}H_8$ formation are mapped out based on ROP analyses at 1500 K in individual cases, as presented in Scheme 2. The formation of $C_{10}H_8$ is dominated by the $C_9H_7CH_2$ dehydrogenation/isomerization and the C_7H_5+C_3H_3 recombination. Besides, the decomposition of benzobicyclo[2,2,2]octatriene (BICYCLO) [51] also has a non-negligible contribution. The relative importance of the mentioned channels varies with the initial fuel compositions. When gradually adding C_2H_2, $C_{10}H_8$ originating from $C_9H_7CH_2$ takes a higher proportion, while the channels through C_7H_5+C_3H_3 recombination and BICYCLO decomposition become less important. This is a consequence of the fact that C_7H_7 dissociation is inhibited by the C_7H_7+C_2H_2 reaction forming indene, as detailed in Section 4.2. Indene concentrations increase significantly, resulting in more $C_9H_7CH_3$ formation through indenyl (C_9H_7) + CH_3 recombination (see Fig. 14(c)). On the other hand, the production of C_7H_5, o-C_6H_4 and C_3H_3 is reduced so that $C_{10}H_8$ formation pathways involving these species become less important. The increase in the $C_9H_7CH_3$ pathway prevails the decrease in the C_7H_5+C_3H_3 and the BICYCLO channels, so a slight increase appears in the peak $C_{10}H_8$

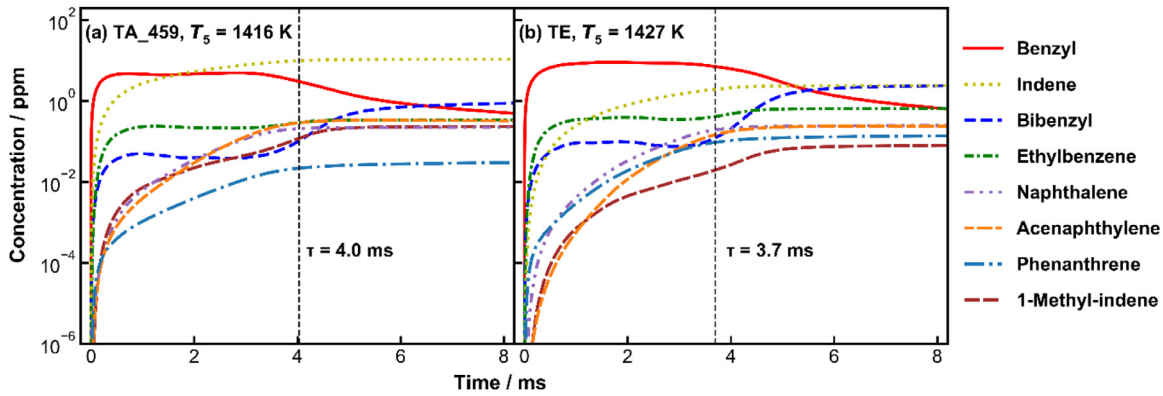

Fig. 13. Simulated species concentrations as a function of time with the measured pressure profiles in (a) TA_459 pyrolysis at T_5 =1416 K; (b) TE pyrolysis at T_5 = 1427 K. The dashed vertical lines indicate the start of quenching.

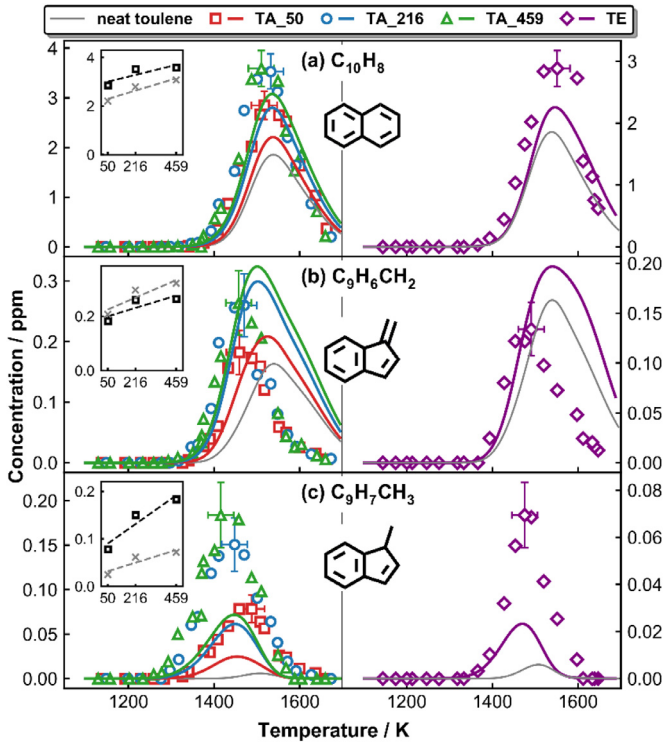

Fig. 14. Experimental (symbols) and modeling (solid lines) concentrations of C_{10} PAH species as a function of the post-shock temperature T_5. The left panel: toluene/C_2H_2 pyrolysis; the upper left insets plot the measured (dark open square) and simulated (gray cross) peak concentrations of separate species against the initial C_2H_2 contents; linear regressions (the dashed lines) of the data points are shown as a visual guide. The right panel: toluene/C_2H_4 pyrolysis. The simulated species concentration profiles in neat toluene pyrolysis (the gray solid lines) are shown as a reference.

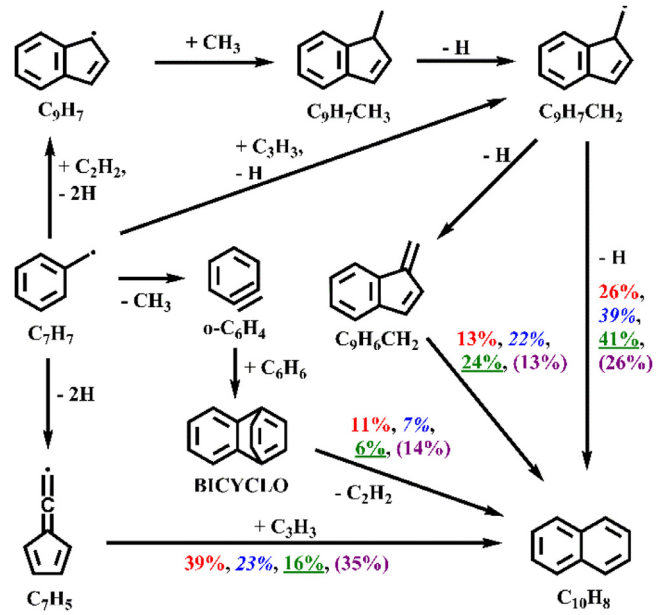

Scheme 2. The reaction pathways leading to naphthalene formation at T_5 of 1500 K in the pyrolysis of toluene/C_2 binary mixtures. The percentage numbers (TA_50: normal; TA_216: italic; TA_459: underlined; TE: in parenthesis) represent the contributions to naphthalene formation by corresponding reactions.

concentration when C_2H_2 is added (see Fig. 14(a)). It is noteworthy that when increasing the amount of C_2H_2, $C_9H_7CH_3$ peak concentrations increase more steeply than those of $C_{10}H_8$ and $C_9H_6CH_2$. This is because $C_9H_7CH_3$ exclusively results from C_9H_7+CH_3 recombination. The $C_9H_6CH_2$ formed through $C_9H_7CH_3$ dehydrogenation increases remarkably with the C_2H_2 addition accordingly, but the other $C_9H_6CH_2$ formation pathway through C_7H_7+C_3H_3 recombination is reduced. This causes a relatively slight growth in $C_9H_6CH_2$ peak concentrations when C_2H_2 is added (see Fig. 14(b)). In the case of toluene/C_2H_4 pyrolysis, since the C_7H_7+C_2H_4 interaction is relatively less efficient in producing indene, the increase in $C_{10}H_8$ formation, which mainly arises from the enhanced C_9H_7 concentration, is less pronounced.

Concentration profiles of major C_{12}–C_{13} PAH species, including acenaphthalene ($C_{12}H_8$), fluorene ($C_{13}H_{10}$) and biphenylmethane ($C_6H_5CH_2C_6H_5$), are shown in Fig. 15. A more obvious increasing trend shows in $C_{12}H_8$ peak concentrations than that in $C_{10}H_8$ peak concentrations when raising the C_2 contents in the fuel mixtures. The formation scheme of $C_{12}H_8$, based on the ROP-analyzed results at 1500 K, is shown in Scheme 3. Three sources are responsible for $C_{12}H_8$ production from toluene/C_2 pyrolysis. The C_9H_7+C_3H_3 recombination and the subsequent dehydrogenation and ring-rearrangement processes are the governing pathway, followed by the stepwise C_2H_2 addition through phenyl (C_6H_5) → phenylacetylene ($C_6H_5C_2H$) → naphthyl ($C_{10}H_7$) (or benzofulvenyl (C_9H_6CH) [34]) → acenaphthalene ($C_{12}H_8$). Besides, a minor fraction (below 10%) of $C_{12}H_8$ is contributed by the isomerization of biphenyl radical ($C_{12}H_9$) through the intermediate cyclopenta[a]indene (BENZO) [51,52]. The relative importance of the major pathways leading to $C_{12}H_8$ is not obviously changed by the varied initial fuel compositions. The two major

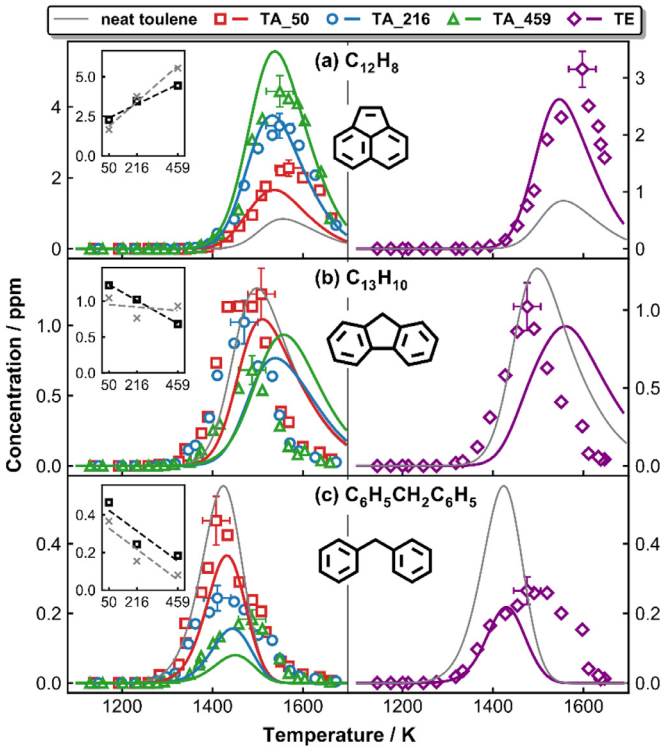

Fig. 15. Experimental (symbols) and modeling (solid lines) concentrations of C_{12}–C_{13} PAH species as a function of the post-shock temperature T_5. The left panel: toluene/C_2H_2 pyrolysis; the upper left insets plot the measured (dark open square) and simulated (gray cross) peak concentrations of separate species against the initial C_2H_2 contents; linear regressions (the dashed lines) of the data points are shown as a visual guide. The right panel: toluene/C_2H_4 pyrolysis. The simulated species concentration profiles in neat toluene pyrolysis (the gray solid lines) are shown as a reference.

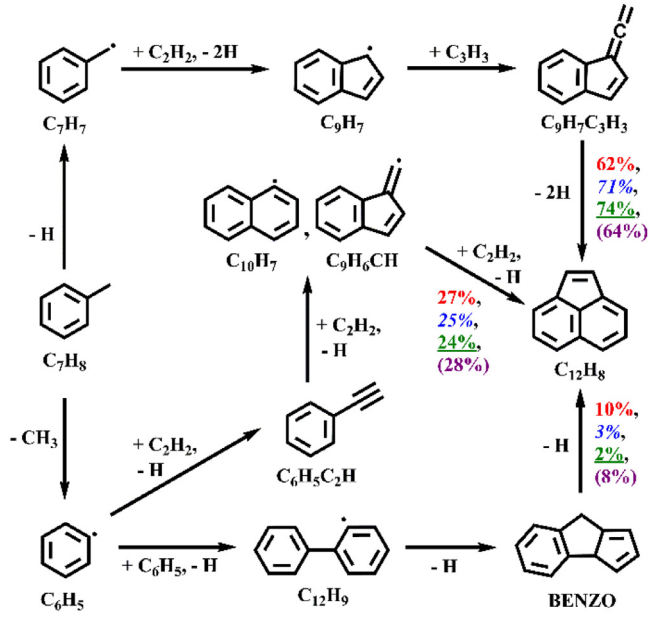

Scheme 3. The reaction pathways leading to acenaphthalene formation at T_5 of 1500 K in the pyrolysis of toluene/C_2 binary mixtures. The percentage numbers (TA_50: normal; TA_216: italic; TA_459: underlined; TE: in parenthesis) represent the contributions to acenaphthalene formation by corresponding reactions.

$C_{12}H_8$ formation pathways, through C_9H_7+C_3H_3 and $C_{10}H_7$ (or C_9H_6CH) +C_2H_2, rely on the production of important precursors, C_9H_7 and $C_6H_5C_2H$, and thus the Hydrogen-Abstraction-C_2H_2-Addition (HACA) steps starting from C_7H_7 and C_6H_5, respectively. Consequently, both pathways are intensified when increasing the C_2H_2 contents in the reaction system. Though the formation of C_3H_3 is reduced due to the inhibited C_7H_7 decomposition, as mentioned above, the level of C_9H_7 is more a limiting factor that influences the efficiency of the C_9H_7+C_3H_3 recombination leading to $C_{12}H_8$ formation. Once again, an addition of about 500 ppm C_2H_4 results in a $C_{12}H_8$ peak concentration falling between those in TA_50 and TA_216, *i.e.*, the cases with 50 ppm and 216 ppm of C_2H_2 addition.

Obvious decreasing trends are present in the peak concentrations of the C_{13} PAH species (see the insets of Fig. 15(b) and (c)). Compared to the case of neat toluene pyrolysis, the presence of C_2H_2 or C_2H_4 impedes the formation of biphenylmethane ($C_6H_5CH_2C_6H_5$), owing to that the predominant pathway through the C_7H_7+C_6H_5 recombination is inhibited by the lowered C_7H_7 level, as addressed above. Meanwhile, the concentrations of C_6H_5 also decrease, as can be noted from the simulated C_6H_5 profiles in Fig. S8 in the *Supplementary Material*. C_6H_5 is mainly produced from toluene unimolecular decomposition (C_7H_8(+M) = C_6H_5+CH_3(+M)) below the temperature where toluene is depleted. An increasing portion of C_6H_5 reacts with C_2H_2 (or C_2H_4) available in the reaction systems when enhancing the initial C_2 fuel contents. Therefore, less C_6H_5 can participate in the recombination reaction with C_7H_7. The reduced concentrations of both precursors, C_7H_7 and C_6H_5, together result in a sharp decrease in $C_6H_5CH_2C_6H_5$ peak concentrations. Nevertheless, the peak concentrations of fluorene ($C_{13}H_{10}$), which mostly comes from $C_6H_5CH_2C_6H_5$ consumption, decrease at a relatively slower rate when introducing C_2 fuels to toluene pyrolysis. This is mainly because H atom concentrations are enhanced by the added C_2 fuels, which facilitates the $C_6H_5CH_2C_6H_5$ consumption through hydrogen abstraction reactions. The resulting radical 2-benzylphenyl ($C_{13}H_{11}$) subsequently decomposes, leading to $C_{13}H_{10}$ formation.

Figure 16 displays the concentration profiles as well as the peak concentration variation trends of three $C_{14}H_{10}$ isomers, namely, phenanthrene ($PC_{14}H_{10}$), anthracene ($AC_{14}H_{10}$) and 9-methylene-fluorene ($C_{13}H_8CH_2$). Peak concentrations of all three isomers decrease with the increased C_2 contents in a similar manner. Reaction pathways leading to the $C_{14}H_{10}$ isomers formation at 1450 K are presented in Scheme 4. The inhibited formation of all three $C_{14}H_{10}$ isomers can be explained by the reduced C_7 radicals in the reaction system, since their formation largely depends on recombination reactions of C_7 radicals. $PC_{14}H_{10}$, the most dominant $C_{14}H_{10}$ isomer, mainly comes from the C_7H_5 self-recombination and $AC_{14}H_{10}$ isomerization at the analyzed temperature. Other reaction channels also contribute to $PC_{14}H_{10}$ formation: the dehydrogenation of hydro-methylene-fluorene radical ($C_{13}H_9CH_2$) that is mainly produced from C_7H_7+C_7H_5 recombination, H-assisted isomerization of $C_{13}H_8CH_2$ and the $C_6H_5C_2H$+C_6H_5 addition-elimination reactions. As discussed in our previous work [38], the $C_6H_5C_2H$+C_6H_5 reactions are important sources of C_{14} PAH species including $PC_{14}H_{10}$ and $C_{13}H_8CH_2$. A total of about 10% $PC_{14}H_{10}$ originates from the $C_6H_5C_2H$ + C_6H_5 reactions at 1450 K, and this proportion slightly increases with the initial C_2H_2 contents, mainly because of the increased $C_6H_5C_2H$ formation, as discussed in Section 4.1. A similar trend is also seen in the $C_{13}H_8CH_2$ formation, to which the reaction $C_6H_5C_2H$+C_6H_5 = $C_{13}H_8CH_2$+H makes an increasing contribution when enhancing the initial C_2H_2 contents, though $C_{13}H_8CH_2$ predominantly comes from $C_{13}H_9CH_2$ dehydrogenation. The current kinetic model, which satisfactorily reproduces the measurements of $AC_{14}H_{10}$, attributes the $AC_{14}H_{10}$ formation to the $CH_3C_6H_4$+C_7H_7 recombination. The ratio

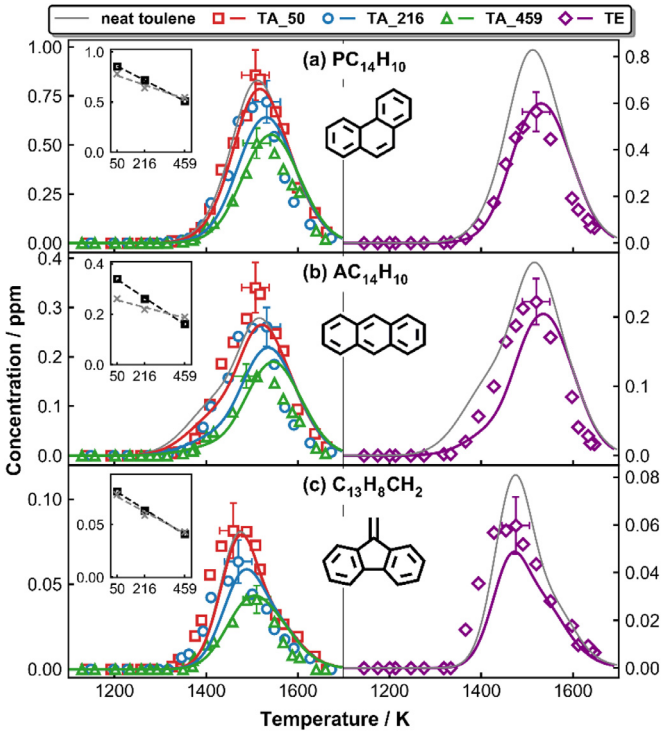

Fig. 16. Experimental (symbols) and modeling (solid lines) concentrations of $C_{14}H_{10}$ PAH isomers as a function of the post-shock temperature T_5. The left panel: toluene/C_2H_2 pyrolysis; the upper left insets plot the measured (dark open square) and simulated (gray cross) peak concentrations of separate species against the initial C_2H_2 contents; linear regressions (the dashed lines) of the data points are shown as a visual guide. The right panel: toluene/C_2H_4 pyrolysis. The simulated species concentration profiles in neat toluene pyrolysis (the gray solid lines) are shown as a reference.

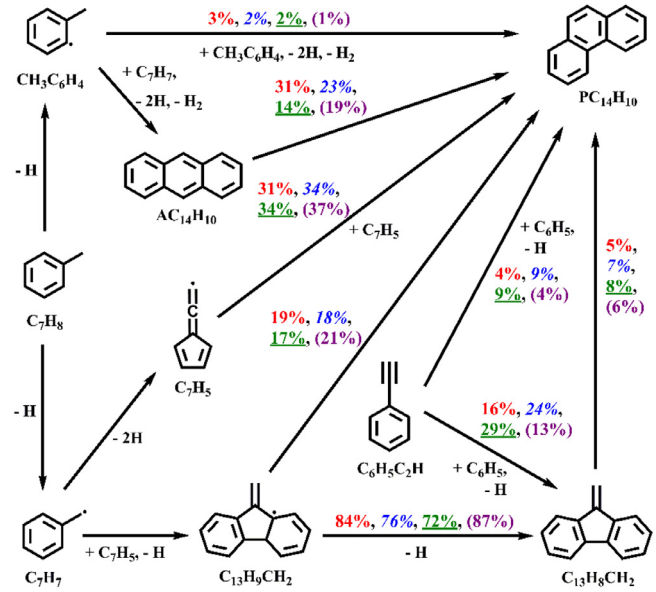

Scheme 4. The reaction pathways leading to the formation of $C_{14}H_{10}$ isomers at T_5 of 1450 K in the pyrolysis of toluene/C_2 binary mixtures. The percentage numbers (TA_50: normal; TA_216: italic; TA_459: underlined; TE: in parenthesis) represent the contributions to $C_{14}H_{10}$ PAH formation by corresponding reactions.

between $PC_{14}H_{10}$ and $AC_{14}H_{10}$ peak concentrations increase when enhancing the initial C_2H_2 concentration in the fuel mixtures (2.5 in TA_05 → 2.8 in TA_216 → 3.2 in TA). This is because when the level of C_7 radicals is lowered by the added C_2 fuels, the formation of both $PC_{14}H_{10}$ and $AC_{14}H_{10}$ through C_7 recombination is limited, but the $PC_{14}H_{10}$ production is supplied by an alternative $C_6H_5C_2H$+C_6H_5 source, while the formation of $AC_{14}H_{10}$ depends solely on the C_7H_7+$CH_3C_6H_4$ recombination.

Trace amounts (below 0.1 ppm) of $C_{16}H_{10}$ isomers, fluoranthene ($FC_{16}H_{10}$) and pyrene ($PC_{16}H_{10}$) are probed from the pyrolysis of toluene/C_2 binary mixtures, and their concentration evolutions with the post-shock temperature T_5 are shown in Fig. 17. In all studied cases, $FC_{16}H_{10}$ is more abundant than $PC_{16}H_{10}$, and for both $C_{16}H_{10}$ isomers, the measured peak concentrations slightly decrease with the added C_2 fuels. The current model can predict the measurements within experimental uncertainties, but shows limitations in capturing the variation trend of $FC_{16}H_{10}$ peak concentrations in the toluene/C_2H_2 pyrolysis experiments. According to the results of ROP analyses, the formation of both $C_{16}H_{10}$ isomers largely depends on C_{10}+C_6 recombination reactions. Besides, the HACA route through phenanthrene radical ($PC_{14}H_9$) + C_2H_2 leads to $C_{16}H_{10}$, while the C_9H_7+C_7H_7 recombination and the subsequent dehydrogenation and isomerization contributes to the $FC_{16}H_{10}$ formation. The mechanism starting from the recombination of the resonantly stabilized radicals C_7H_7 and C_9H_7 was proposed by Sinha and Raj [19] to account for the formation of four-ring PAHs including both $PC_{16}H_{10}$ and $FC_{16}H_{10}$. It is found that such processes mainly lead to $FC_{16}H_{10}$ under the currently investigated conditions.

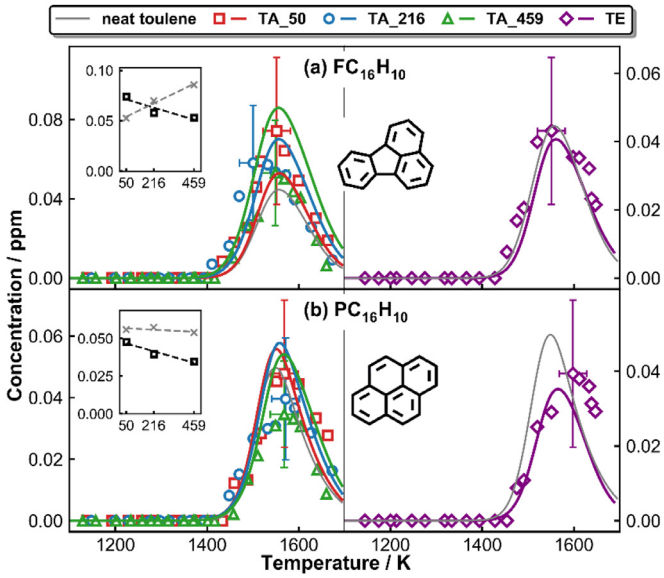

Fig. 17. Experimental (symbols) and modeling (solid lines) concentrations of $C_{16}H_{10}$ PAH isomers as a function of the post-shock temperature T_5. The left panel: toluene/C_2H_2 pyrolysis; the upper left insets plot the measured (dark open square) and simulated (gray cross) peak concentrations of separate species against the initial C_2H_2 contents; linear regressions (the dashed lines) of the data points are shown as a visual guide. The right panel: toluene/C_2H_4 pyrolysis. The simulated species concentration profiles in neat toluene pyrolysis (the gray solid lines) are shown as a reference.

To reveal the potential reason for the contradictory variation trends in the measured and simulated $FC_{16}H_{10}$ peak concentrations, sensitivity analyses for $FC_{16}H_{10}$ are performed in toluene/C_2H_2 pyrolysis at 1550 K. The results are presented in Fig. 18: when raising the initial C_2H_2 contents, reactions along the C_9H_7+C_7H_7 pathway [19] (highlighted in red) play an increasingly important role regarding the $FC_{16}H_{10}$ formation. This is owing to the remarkably enhanced C_9H_7 concentrations when C_2H_2 is added, as previously discussed. On the other hand, C_6H_5 concentrations are reduced, and as a result, the alternative $FC_{16}H_{10}$

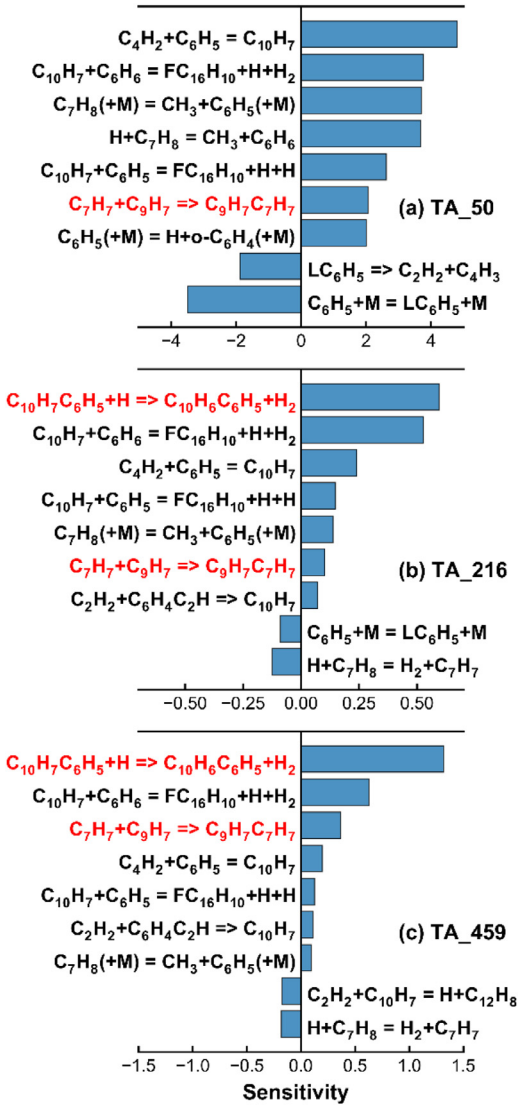

Fig. 18. Sensitivity analyses for fluoranthene ($FC_{16}H_{10}$) in the pyrolysis of toluene/C_2H_2 mixtures at T_5 = 1550 K. (For interpretation of the references to color in this figure, the reader is referred to the web version of this article.)

formation pathways through C_{10}+C_6 recombination becomes less important. The inaccurate prediction for the measured variation trend of $FC_{16}H_{10}$ peak concentrations may come from the inappropriate relative importance of the C_9+C_7 and C_{10}+C_6 channels in the kinetic model, as they are influenced in opposite manners when increasing the initial C_2H_2 contents. In order to better characterize $FC_{16}H_{10}$ formation in different chemical environments, more accurate kinetic description for the mentioned reactions are highly desired, in particular, for the C_{10}+C_6 channels that are expressed as lumped reactions in the kinetic model. Larger PAHs, such as benzo[a]anthracene and chrysene, are also detected at trace levels in the current experiments, but no reliable concentration profiles can be obtained due to the potential condensation in the injection system and lines and the unknown calibration factors. Future kinetic studies on the formation of these heavier PAH compounds are warranted.

5. Conclusions

In this work, a systematic experimental and kinetic modeling work is carried out to highlight the interactions between toluene and C_2 hydrocarbons (C_2H_2 and C_2H_4) under high-pressure pyrolysis conditions. Shock tube experiments are conducted with highly argon diluted binary toluene/C_2H_2 (or C_2H_4) mixtures at a nominal pressure of 20 bar over 1150−1650 K. Given the more pronounced effects of C_2H_2, three toluene/C_2H_2 mixtures with different C_2H_2 concentrations and one toluene/C_2H_4 mixture are used in the experiments. Chemical compositions of the post-shock mixtures are sampled and analyzed through GC/GC–MS technique with high sensitivity. A kinetic model is developed by incorporating interactions between toluene radicals and C_2 fuels. The model can well predict concentration measurements for species ranging from fuels to trace (0.1 ppm level) PAHs in individual studied cases. Moreover, it can successfully capture the variation trends of most species among the different experimental sets. High-fidelity data sets, joined by modeling analyses, are employed to reveal the altered reaction schemes when varying the initial fuel compositions. Strong interactions are noted between benzyl and C_2 fuels, especially C_2H_2, and more specifically, through the C_7H_7+C_2H_x = C_9H_{6+x} + H reactions. Direct effects from such interactions cover three aspects: i) synergistically improved decomposition reactivity is observed for both fuel components, owing to the abundant H atoms generated from the C_7H_7+C_2H_x reactions; ii) C_9 aromatics are largely produced in the binary mixture pyrolysis. Indene (C_9H_8) is identified as the predominant C_9 species, and its peak concentrations steeply increase with the initial C_2H_2 contents. Other C_9 species, such as propynyl (or propenyl) -benzene and ethynyl (or vinyl) -toluene, are also observed, indicating that the other toluene fuel radical, $CH_3C_6H_4$, also reacts with the C_2 fuels; iii) the formation of bibenzyl through benzyl recombination is obviously hindered, since a large portion of benzyl reacts with the extra C_2 in the reaction system. More importantly, we illustrate the effects of the added C_2 fuels on the formation of two- to four-ring PAH species. When enhancing the initial C_2H_2 concentrations, for the PAHs originating from reactions involving indenyl, such as naphthalene, methylindene and acenaphthalene, the peak concentrations clearly increase. Differently, peak concentrations of some other PAH species, such as biphenylmethane, fluorene and phenanthrene, show declining trends, because their formation is governed by reactions of C_7 radicals. For most PAH species, an addition of about 500 ppm C_2H_4 brings an equivalent effect to that of adding C_2H_2 at a specific amount between 50 and 216 ppm.

Declaration of Competing Interest

The authors declare that they have no known competing financial interests or personal relationships that could have appeared to influence the work reported in this paper.

Acknowledgments

This project has received funding from the European Research Council (ERC) under the European Union's Horizon 2020 research and innovation program (grant agreement No. 756785).

Supplementary materials

Supplementary material associated with this article can be found, in the online version, at doi:10.1016/j.combustflame.2020.11.044.

References

[1] S.M. Sarathy, A. Farooq, G.T. Kalghatgi, Recent progress in gasoline surrogate fuels, Prog. Energy Combust. Sci. 65 (2018) 67–108.
[2] D. Davidson, B. Gauthier, R. Hanson, Shock tube ignition measurements of iso-octane/air and toluene/air at high pressures, Proc. Combust. Inst. 30 (2005) 1175–1182.

[3] S.S. Vasu, D.F. Davidson, R.K. Hanson, Shock-tube experiments and kinetic modeling of toluene ignition, J. Propuls. Power 26 (2010) 776–783.
[4] S. Davis, H. Wang, K. Breinsky, C. Law, Laminar flame speeds and oxidation kinetics of benene-air and toluene-air flames, Symp. (Int.) Combust. 26 (1996) 1025–1033.
[5] P. Dagaut, G. Pengloan, A. Ristori, Oxidation, ignition and combustion of toluene: experimental and detailed chemical kinetic modeling, Phys. Chem. Chem. Phys. 4 (2002) 1846–1854.
[6] R. Bounaceur, I. Da Costa, R. Fournet, F. Billaud, F. Battin-Leclerc, Experimental and modeling study of the oxidation of toluene, Int. J. Chem. Kinet. 37 (2005) 25–49.
[7] W. Yuan, Y. Li, P. Dagaut, J. Yang, F. Qi, Investigation on the pyrolysis and oxidation of toluene over a wide range conditions. I. Flow reactor pyrolysis and jet stirred reactor oxidation, Combust. Flame 162 (2015) 3–21.
[8] Y. Li, J. Cai, L. Zhang, T. Yuan, K. Zhang, F. Qi, Investigation on chemical structures of premixed toluene flames at low pressure, Proc. Combust. Inst. 33 (2011) 593–600.
[9] Z. Tian, W.J. Pitz, R. Fournet, P.-.A. Glaude, F. Battin-Leclerc, A detailed kinetic modeling study of toluene oxidation in a premixed laminar flame, Proc. Combust. Inst. 33 (2011) 233–241.
[10] R. Sivaramakrishnan, R. Tranter, K. Brezinsky, A high pressure model for the oxidation of toluene, Proc. Combust. Inst. 30 (2005) 1165–1173.
[11] R. Sivaramakrishnan, R.S. Tranter, K. Brezinsky, High pressure pyrolysis of toluene. 1. Experiments and modeling of toluene decomposition, J. Phys. Chem. A 110 (2006) 9388–9399.
[12] W. Sun, A. Hamadi, S. Abid, N. Chaumeix, A. Comandini, Probing PAH formation chemical kinetics from benzene and toluene pyrolysis in a single-pulse shock tube, Proc. Combust. Inst. (2020), doi:10.1016/j.proci.2020.1006.1077.
[13] G. da Silva, J.W. Bozzelli, The C7H5 fulvenallenyl radical as a combustion intermediate: potential new pathways to two- and three-ring PAHs, J. Phys. Chem. A 113 (2009) 12045–12048.
[14] A. Matsugi, A. Miyoshi, Computational study on the recombination reaction between benzyl and propargyl radicals, Int. J. Chem. Kinet. 44 (2012) 206–218.
[15] A. Matsugi, A. Miyoshi, Reactions of o-benzyne with propargyl and benzyl radicals: potential sources of polycyclic aromatic hydrocarbons in combustion, Phys. Chem. Chem. Phys. 14 (2012) 9722–9728.
[16] S. Sinha, A. Raj, Polycyclic aromatic hydrocarbon (PAH) formation from benzyl radicals: a reaction kinetics study, Phys. Chem. Chem. Phys. 18 (2016) 8120–8131.
[17] A.M. Mebel, Y. Georgievskii, A.W. Jasper, S.J. Klippenstein, Pressure-dependent rate constants for PAH growth: formation of indene and its conversion to naphthalene, Faraday Discuss 195 (2017) 637–670.
[18] L. Vereecken, J. Peeters, Reactions of chemically activated C 9 H 9 species II: the reaction of phenyl radicals with allene and cyclopropene, and of benzyl radicals with acetylene, Phys. Chem. Chem. Phys. 5 (2003) 2807–2817.
[19] S. Sinha, R.K. Rahman, A. Raj, On the role of resonantly stabilized radicals in polycyclic aromatic hydrocarbon (PAH) formation: pyrene and fluoranthene formation from benzyl–indenyl addition, Phys. Chem. Chem. Phys. 19 (2017) 19262–19278.
[20] G.B. Skinner, E.M. Sokoloski, Shock tube experiments on the pyrolysis of ethylene, J. Phys. Chem. 64 (1960) 1028–1031.
[21] M. Frenklach, S. Taki, M. Durgaprasad, R. Matula, Soot formation in shock-tube pyrolysis of acetylene, allene, and 1, 3-butadiene, Combust. Flame 54 (1983) 81–101.
[22] M. Frenklach, D.W. Clary, W.C. Gardiner Jr, S.E. Stein, Detailed kinetic modeling of soot formation in shock-tube pyrolysis of acetylene, Symp. (Int.) Combust. 20 (1985) 887–901.
[23] C. Wu, H. Singh, R. Kern, Pyrolysis of acetylene behind reflected shock waves, Int. J. Chem. Kinet. 19 (1987) 975–996.
[24] Y. Hidaka, K. Hattori, T. Okuno, K. Inami, T. Abe, T. Koike, Shock-tube and modeling study of acetylene pyrolysis and oxidation, Combust. Flame 107 (1996) 401–417.
[25] M. Ruiz, A. Callejas, A. Millera, M. Alzueta, R. Bilbao, Soot formation from C2H2 and C2H4 pyrolysis at different temperatures, J. Anal. Appl. Pyrolysis 79 (2007) 244–251.
[26] N. Sánchez, A. Callejas, A. Millera, R. Bilbao, M. Alzueta, Formation of PAH and soot during acetylene pyrolysis at different gas residence times and reaction temperatures, Energy 43 (2012) 30–36.
[27] C. Saggese, N.E. Sánchez, A. Frassoldati, A. Cuoci, T. Faravelli, M.U. Alzueta, E. Ranzi, Kinetic modeling study of polycyclic aromatic hydrocarbons and soot formation in acetylene pyrolysis, Energy Fuels 28 (2014) 1489–1501.
[28] I. Gay, R. Kern, G. Kistiakowsky, H. Niki, Pyrolysis of ethylene in shock waves, J. Chem. Phys. 45 (1966) 2371–2377.
[29] Y. Hidaka, T. Nishimori, K. Sato, Y. Henmi, R. Okuda, K. Inami, T. Higashihara, Shock-tube and modeling study of ethylene pyrolysis and oxidation, Combust. Flame 117 (1999) 755–776.
[30] Y. Yoshizawa, H. Kawada, M. Kurokawa, A shock-tube study on the process of soot formation from acetylene pyrolysis, Symp. (Int.) Combust. 17 (1979) 1375–1381.
[31] T. Kruse, P. Roth, Kinetics of C2 reactions during high-temperature pyrolysis of acetylene, J. Phys. Chem. A 101 (1997) 2138–2146.
[32] M. Frenklach, H. Wang, Detailed modeling of soot particle nucleation and growth, Symp. (Int.) Combust. 23 (1991) 1559–1566.
[33] H. Wang, M. Frenklach, Calculations of rate coefficients for the chemically activated reactions of acetylene with vinylic and aromatic radicals, J. Phys. Chem. 98 (1994) 11465–11489.
[34] A.M. Mebel, Y. Georgievskii, A.W. Jasper, S.J. Klippenstein, Temperature-and pressure-dependent rate coefficients for the HACA pathways from benzene to naphthalene, Proc. Combust. Inst. 36 (2017) 919–926.
[35] B. Shukla, A. Susa, A. Miyoshi, M. Koshi, In situ direct sampling mass spectrometric study on formation of polycyclic aromatic hydrocarbons in toluene pyrolysis, J. Phys. Chem. A 111 (2007) 8308–8324.
[36] A. Matsugi, A. Miyoshi, Modeling of two-and three-ring aromatics formation in the pyrolysis of toluene, Proc. Combust. Inst. 34 (2013) 269–277.
[37] T. Li, Y. Zhang, W. Yuan, C. Cao, W. Li, J. Yang, Y. Li, Unraveling synergistic effects on pyrolysis reactivity and indene formation in co-pyrolysis of toluene and acetylene, Proc. Combust. Inst. (2020), doi:10.1016/j.proci.2020.1006.1176.
[38] W. Sun, A. Hamadi, S. Abid, N. Chaumeix, A. Comandini, An experimental and kinetic modeling study of phenylacetylene decomposition and the reactions with acetylene/ethylene under shock tube pyrolysis conditions, Combust. Flame 220 (2020) 257–271.
[39] W. Sun, A. Hamadi, S. Abid, N. Chaumeix, A. Comandini, A comparative kinetic study of C8–C10 linear alkylbenzenes pyrolysis in a single-pulse shock tube, Combust. Flame 221 (2020) 136–149.
[40] A. Comandini, T. Malewicki, K. Brezinsky, Online and offline experimental techniques for polycyclic aromatic hydrocarbons recovery and measurement, Rev. Sci. Instrum. 83 (2012) 034101.
[41] J.A. Manion, I.A. Awan, A shock tube study of H atom addition to cyclopentene, Int. J. Chem. Kinet. 50 (2018) 225–242.
[42] H. Jin, L. Xing, J. Hao, J. Yang, Y. Zhang, C. Cao, Y. Pan, A. Farooq, A chemical kinetic modeling study of indene pyrolysis, Combust. Flame 206 (2019) 1–20.
[43] M. Colket, D. Seery, Reaction mechanisms for toluene pyrolysis, Symp. (Int.) Combust. 25 (1994) 883–891.
[44] W. Pejpichestakul, E. Ranzi, M. Pelucchi, A. Frassoldati, A. Cuoci, A. Parente, T. Faravelli, Examination of a soot model in premixed laminar flames at fuel-rich conditions, Proc. Combust. Inst. 37 (2019) 1013–1021.
[45] A. Burcat, B. Ruscic, Third Millenium ideal gas and condensed phase thermochemical database for combustion (with update from active thermochemical tables), Argonne National Laboratory Argonne, IL, 2005.
[46] COSILABThe combustion simulation laboratory, Rotexo GmbH & Co., KG, Haan, Germany, 2009 Version 3.3.2..
[47] W. Tang, K. Brezinsky, Chemical kinetic simulations behind reflected shock waves, Int. J. Chem. Kinet. 38 (2006) 75–97.
[48] X. Han, J.M. Mehta, K. Brezinsky, Temperature approximations in chemical kinetics studies using single pulse shock tubes, Combust. Flame 209 (2019) 1–12.
[49] J.A. Manion, D.A. Sheen, I.A. Awan, Evaluated kinetics of the reactions of H and CH3 with n-alkanes: experiments with n-butane and a combustion model reaction network analysis, J. Phys. Chem. A 119 (2015) 7637–7658.
[50] L.A. Mertens, I.A. Awan, D.A. Sheen, J.A. Manion, Evaluated site-specific rate constants for reaction of isobutane with H and CH3: shock tube experiments combined with bayesian model optimization, J. Phys. Chem. A 122 (2018) 9518–9541.
[51] A. Comandini, T. Malewicki, K. Brezinsky, Chemistry of polycyclic aromatic hydrocarbons formation from phenyl radical pyrolysis and reaction of phenyl and acetylene, J. Phys. Chem. A 116 (2012) 2409–2434.
[52] B. Shukla, K. Tsuchiya, M. Koshi, Novel products from C6H5+ C6H6/C6H5 reactions, J. Phys. Chem. A 115 (2011) 5284–5293.